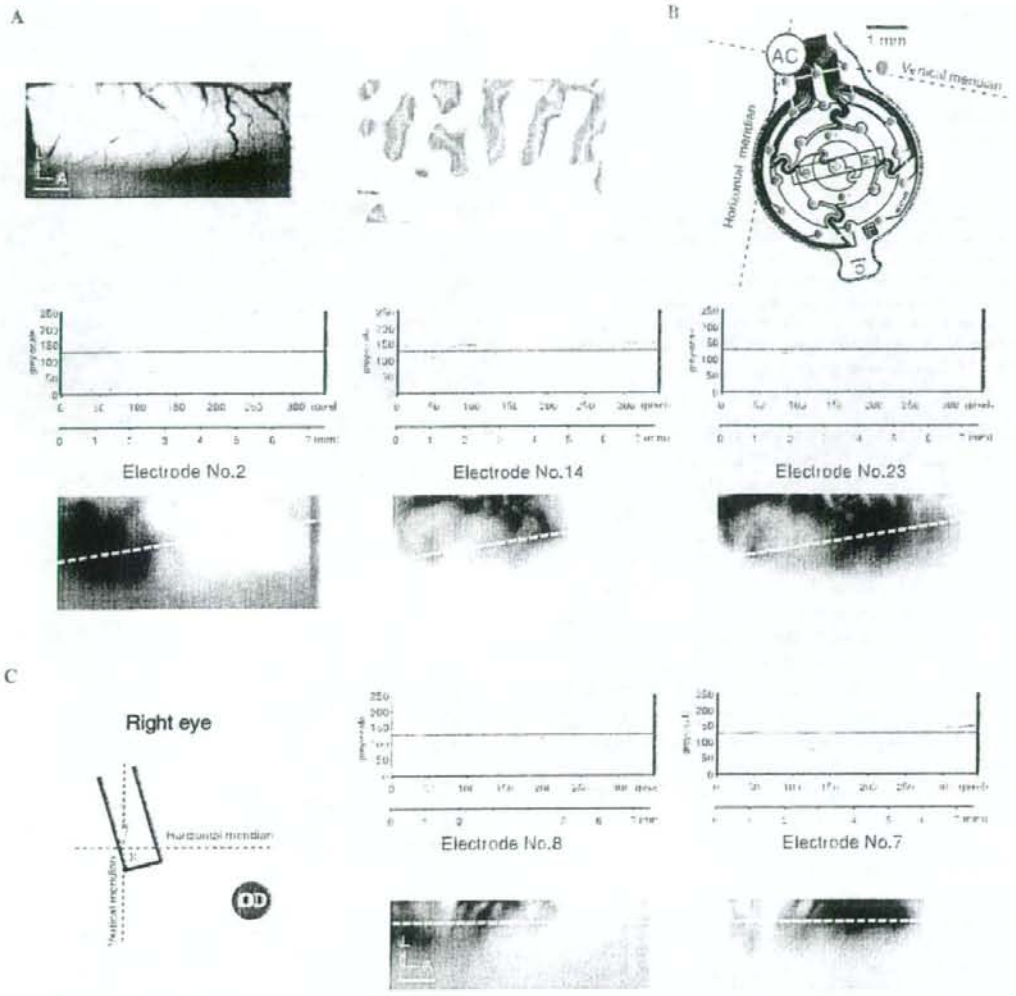


Fig. 3. Optically recorded cortical activations by visual (A), electrical epi- (B), and sub-retinal (C) stimulation with neighboring retinal electrodes. (A) Visual stimulation through a stationary horizontally oriented slit (0,5° width, 40° length) with a moving grating (see Section 2) positioned at vertical retinal eccentricities (elevation) corresponding (from left to right) to the electrode positions 2, 14, 23 in (B). The optical recordings demonstrate the spread and retinotopic displacement of visually evoked cortical activation profiles in cat area 18 (SCMs, see Section 2). (B and C) Optically recorded activation profiles (SCMs) during stimulation with spatially displaced retinal electrodes. Graphs above each optical image show one dimensional activation profiles transformed from the intensity (gray scale) levels along the broken lines (minima represent maximal activation). Considerable cortical activation is represented by the darkest black spots. They move successively from left to right with visual and electrical stimuli and are of similar size with visual and electrocal stimuli. Differences are mainly due to the long slit visual and the focal electrical stimulation. The optical images show responses to stimulation of neighboring electrodes separated by 750 μm (epi-retinal, (B); stimulation current: ±150 μA, 250 μs for each phase) and 330 μm (sub-retinal, (C); stimulation current: ±50 μA, 1 ms for each phase), and reveal activity shifts up to 3,7 mm along the anterior–posterior axis of the cortex (B). Importantly, the cortical magnification factor decreases about exponentially with increasing distance from the projection of the area centralis, and the shifts of the activated cortical locations correspond well to the published retinotopic maps (Tusa et al. 1978; Tusa et al. 1979). The exact position of the stimulation electrodes resulting in the activity images in (B and C) are shown in corresponding insets. Scale bars at optical images 1 mm in (A–C). L, lateral, A, anterior.

analyzed. Fig. 4A shows example montages in which the averaged population responses in the optic tract to single site stimulation are plotted together with the applied current amplitudes. Two important facts are demonstrated here. First, the currents for evoking similar response amplitudes differ by a factor of up to ~20 (from ±4 to ±78 μA;

Table 1
Spatial resolutions obtained with epi- and sub-retinal stimulation

| Cortical recording | Epi-retinal stimulation | Sub-retinal stimulation |
|---|---|---|
| Optical | 2.50° (thin-film electrodes) | 2.50° (thin-film electrodes) |
| Microelectrode array | 0.68° (cone electrodes) | |
| Microelectrode array | 1.20° (thin-film electrodes) | 0.90° (thin-film electrodes)<br>1.30° (thin-film electrodes) |

The spatial resolution for microelectrode array recordings represents the resolution of the primary response. The lower resolution obtained with optical recordings corresponds well to the spatial resolution of the late responses of microelectrode recordings (see text). The high resolution of 0.68° with epi-retinal stimulation were not obtained with currently available and implantable electrode arrays but with singly in the eye inserted microelectrodes having cone-shaped tips.

epi-retinal stimulation). Second, the response delays (2–3 ms) and their durations (1–2 ms) are very short, indicating that the electrical impulses activate ganglion cells directly and evoke only a single spike per neuron (with epi- and sub-retinal stimulation, Fig. 4A). Fig. 4B shows responses to short light flashes recorded for comparison with the same optic tract electrodes. The composite visually and electrically evoked field responses were observed in a range of 30–200 μV. Compared with the responses to electrical stimuli (delay: 2–3 ms, duration: 1 ms) the visual responses have much longer latencies (~20 ms) and duration (20–35 ms) as is typical for visual population responses in the optic tract to which single ganglion cells generally contribute sequences of several spikes at a broad range of delays and with a higher degree of jitter compared to electrical impulse activation.

### 3.3. Activation of cortical neurons

#### 3.3.1. Temporal precision of primary cortical action potentials

Retinal electrical stimuli evoked single impulses in ganglion cells with a repetition jitter of <1 ms (Figs. 4 and 5). Because signal transmission across geniculate synapses is highly stable in the applied frequency range of electrical stimulation (Eysel, Grüsser, & Pecci Saavedra, 1974) effective activation volleys will arrive at the primary cortical synapses also with low temporal jitter. Hence, primary cortical spikes can also be generated with high temporal precision. This is demonstrated in Fig. 5. The retino-cortical delay for the first evoked spike in this example is about 6 ms with a jitter <1 ms. For a given cortical recording location, delay and jitter depend on stimulation current and electrode type. The stronger the retinal activation the shorter the latency and the less variable the response. Fig. 5 also shows a pause after the primary spikes of about 2 ms followed by a less precise second spike. We cannot decide on our present data whether the second spikes are due to a primary activation by parvo- or konio-cellular afferents or whether they are secondary spikes in response to magnocellular input (for comparison of these cell types, see: Xu, Ichida, Allison, Bonds, & Casagrande, 2001). In summary, our results show that the visual pathway, from electrical stimulation of retinal ganglion cells to the primary responses in visual cortex, shows a high temporal precision,

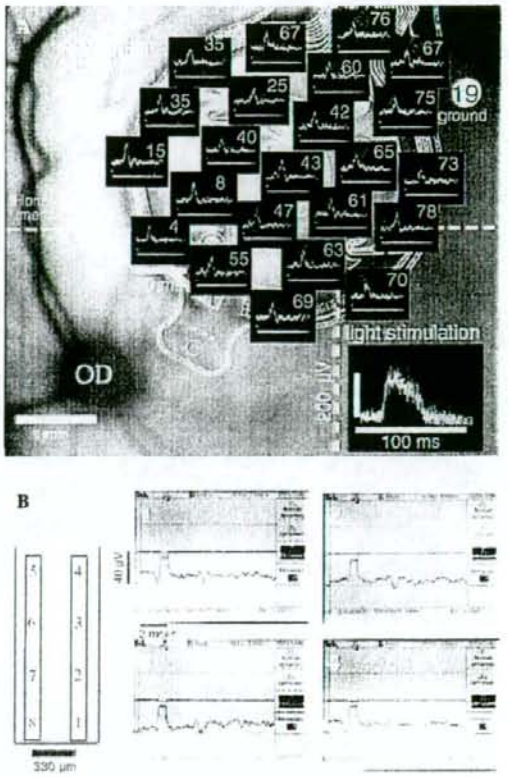


Fig. 4. Epi- and sub-retinal stimulation with thin-film electrodes and population spike recordings from the optic tract. (A) Image of the retinal implant (inter-electrode distance 750 μm) in the upper nasal quadrant of the retina overlapping area centralis. Schematic montage of thin-film array in front of retinal background superimposed by average response waveforms (small insets) evoked by short, single biphasic stimuli (±4 to ±78 μA; balanced current; waveform: 250 μs negative; 250 μs off; 250 μs positive) delivered at 1 Hz via single electrodes of the implant against ground (19). Optic tract recordings were made with a concentric bipolar tungsten electrode (SNEX-100, Rhodes Medical, Woodland Hills, CA, USA). For positioning of the recording electrode and comparison to electrical stimulation, recordings were made during 1 Hz stroboscopic light stimulation (lower right inset). Note the difference in the latency from stimulus onset to the peak responses for optical (about 20 ms) and electrical stimulation (about 2.5 ms). OD: optic disk. (B) Position of the dual in line thin-film array relative to area centralis (case S-R.02) is shown to the left. The tip of the array (electrodes 1, 8) covered the foveal zone whereas the other electrodes extended along the vertical meridian in the upper hemi-retina (inter-electrode distance 330 μm). Evoked potentials to electrical stimulation (50 μA, biphasic current pulses, averaged response to 128 identical repetitions) delivered by electrodes 1, 2, 3, and 4, respectively, against the combined electrodes 5–8 of the implant as ground. Please note the slightly longer latency (about 3 ms) after sub-retinal in comparison to epi-retinal electrical stimulation.

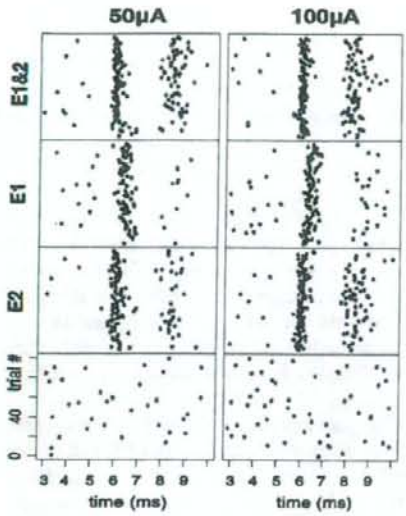


Fig. 5. Variability of cortical single unit spike responses to single site epi-retinally applied impulse-pairs (2 × 0.2 ms at 50µA (A) and 100µA (B)). The raster plots of 32 identical stimulus repetitions show from top to bottom: retinal stimulation via cone electrodes E1 and E2 synchronously, E1 and E2 separately, and maintained activity (no stimulation). Note the short retino-cortical activation delays of ~6 ms for the first spikes. Note also that the higher stimulus current (B) and the synchronous stimulation of E1 and E2 (A, B top row) lead to higher numbers of spikes and reduced temporal jitter.

because the relatively slow retinal input stages (phototransduction, synaptic transmission in the retinal network) are not in use. However, temporal resolution in visual perception should also be limited by the temporal properties of cortical circuits. These upper limits can be estimated from the time courses of cortical population responses (MUA, LFP) to electrical retinal impulse stimuli.

### 3.3.2. Resolution from signal approach

One coarse method for estimating the temporal resolution from the cortical responses is the measurement of the response duration at a certain amplitude (e.g., 10% of maximum). Figs. 1 and 2 (inset) show a variety of cortical peristimulus time histograms (PSTHs) in response to repetitions of single electrical impulses. In these examples, response durations are about 40–100 ms corresponding to an upper frequency limit of about 25–10 Hz. It is known that the retino-cortical pathway changes its temporal transfer properties with the rate of stimulation. This was found with stimulus patterns (Gamma interval distributions) which were systematically varied in their average impulse rates between 1 and 80 imp/s (Eger et al., 2005; Wilms et al., 2003).

Table 2 shows the average values of temporal resolutions obtained with epi- and sub-retinal stimulation. The types of electrodes, two-dimensional thin-film and three-dimensional cone-shaped stimulation electrodes revealed about the same values. Temporal resolutions with sub-retinal stimulation are only slightly lower compared to those

Table 2
Temporal resolutions for focal epi- and sub-retinal stimuli obtained from cortical microelectrode recordings, estimated directly from response time courses of microelectrode recordings (LFP)

| Cortical recording | Epi-retinal stimulation | Sub-retinal stimulation |
|---|---|---|
| Microelectrode array | 33 ms or 30/s (cone electrodes) | 40 ms or 25/s (thin-film electrode) |
| Microelectrode array | 33 ms or 30/s (thin-film electrode) | 45 ms or 22/s (thin-film electrode) |

The temporal resolution is derived from the duration of the activation period t/ms and is also expressed in possible frames/s (1000/activation period).

with epi-retinal stimulation. This might be due to the longer and slower retinal pathway including bipolar and ganglion cells with the sub-retinal activations while epi-retinal stimulation directly activate ganglion cells.

As the results for temporal resolutions in Table 2 were derived from averaged responses and therefore do not reveal the variability of responses to single stimuli we chose another approach. Here, we have applied information theory that can capture the amount of stimulus–response information by taking the variability of cortical responses to single impulses quantitatively into account.

### 3.3.3. Resolutions from information approach

The rate of information, transmitted by a stimulus train with Gamma interval distribution (Eger et al., 2005) to a single cortical recording site was calculated for identical sequences of focal light flashes and electrical impulses applied to the same retinal site. Patterns of light flashes at rates between 2 and 10 Hz show a maximum of transmitted information of about 20–40 bit/s. At high flash rates (20–50 Hz) transmission of information steeply declined, probably due to the retinal high frequency cut-off above 10 Hz (e.g., Shapley & Victor, 1981). While most of the LFP recordings showed a clear maximum, this was only the case in few MUA recordings, most likely due to the different spatial ranges contributing to an LFP and MUA recording. With stochastic stimulus sequences striking differences between electrical and visual stimulation were observed. First, in contrast to visual stimulation (with a spread of information across several recording locations) electrical stimulation delivered high rates of information only to single focal cortical patches (input range of a single cortical recording location) with very little information spread towards neighboring cortical locations. Second, using electrical stimulation and cortical LFP recordings, information rates increased continuously in parallel with stimulation rates up to the highest applied rate of 80 Hz (details in Eger et al., 2005) whereas they showed a peak at 4–8 Hz flash rates when visual stimuli were applied.

## 4. Discussion

The most important results are the relatively high spatial and temporal resolutions obtained with electrical retina activations in the visual cortex: about 1° visual angle (Table 1)

and 25 Hz (Table 2). Epi-and sub-retinal stimulation revealed similar results. As our resolution estimates were derived from recordings in primary visual cortex, there are good reasons to believe that they can directly be related to visual perception in the blind with retinal implants, as is argued below.

### 4.1. Spatial resolution

Spatial resolution was estimated on the basis of the retino-cortical spread of activation in response to a focal electrical stimulation of the retina (Table 1). We transformed this retino-cortical point spread function to degrees of visual angle in visual space at a reference eccentricity of 2° (see Section 2; assumed average electrode eccentricity of retinal implants). From the point of view of human application the cortical activation spread is an important measure because it is directly related to the spatial extent of perceived phosphenes, and cortical neurons outside the activation range, not coupled to the focal stimulus, will thus not contribute to perception. The cortical activation spread, on the other hand, may underestimate the actually obtainable spatial resolution, because stimulation with focal visual stimuli results in comparable cortical distributions of activity (Fig. 3A; see also Grinvald, Lieke, Frostig, & Hildesheim, 1994) and are associated with visual perceptions of much higher resolutions.

With the current technology of retinal stimulation, we could not activate individual ganglion cells in isolation by a single electrical impulse, instead we evoked near-synchronized responses from a spatially circumscribed population of cells in the retina. Each activated ganglion cell contributed only with a single spike to epi- and sub-retinal impulse stimuli (Figs. 4 and 5). In contrast to this, in the isolated chick retina, sub-retinal single impulse stimuli evoked groups of action potentials in retinal ganglion cells (Stett et al., 2000). The spatial resolution derived from these in vitro experiments was between 50 and 100 μm on the retina and corresponded to a retinal spatial resolution of 0.3–0.5°, as has been shown in rats suffering from complete retinal degeneration as well (RCS-rats) by the same technology.

Quite importantly, we could not differentiate which types and combination of types of retinal ganglion cells were activated, i.e., on- or off-center, magno-, parvo- or konio-cellular neurons (for cell types, see: Nirenberg, Carcieri, Jacobs, & Latham, 2001; Waessle & Boycott, 1991). We assume, however, that all types contributed to the population responses. This may render vision transmitted by such arrays as color-less since the S-, M-, and L-cone systems would be activated simultaneously. This has experimentally been confirmed with epi-retinal stimulation in human subjects evoking phosphenes that were reported as *bright*, not *dark* (Humayun et al., 1999). It also implies that we were not able to activate the retino-cortical network with electrical stimulation in the same way as with visual stimuli. Accordingly, with electrical stimulation, local contrasts will probably be processed at lower spatial and intensity resolutions than are obtained with visual stimuli in the intact system. In addition, perceptual resolutions may not adequately be estimated by the activity distributions obtained by extracellular microelectrode recordings of LFP and optical imaging signals. Both types of signals are correlated with the local superpositions of post-synaptic potentials without significant contributions from action potentials (Grinvald et al., 1994; Grinvald et al., 1999; Mitzdorf, 1987). Excitatory and inhibitory neurons contribute to these signals and it remains unclear how they are precisely related to perceptual resolution. The spatial resolutions calculated from the width of cortical activation profiles after electrical stimulation in the anesthetized cat retina should therefore be taken as a conservative approach most probably underestimating the obtainable perceptual spatial resolution in humans.

The smallest cortical activation profiles were represented by the early cortical components (10–20 ms) in response to the afferent input volley (layers 4 and 6 in area 17; Fig. 1). Previous work showed that early cortical components evoked by visual stimuli (30–50 ms post-stimulus) code local visual properties, including contour orientation, contrast and movement direction (Eckhorn, Frien, Bauer, Woelbern, & Kehr, 1993; Shevelev, Eysel, Lazareva, & Sharaev, 1998), while later components are mainly influenced by cortico-cortical interactions representing visual context (Gail, Brinksmeyer, & Eckhorn, 2000; Lamme, Rodriguez-Rodriguez, & Spekreijse, 1999). Correspondingly, later cortical responses to electrical stimulation are probably dominated by cortico-cortical lateral and feedback interactions from outside the classical RF (Angelucci et al., 2002; Bullier et al., 2001), which explains the observed dynamic expansion of the activation spread by factors of 2 to 3 during the later 50–100 ms of the response profiles (Fig. 1; see also Wilms et al., 2003). This might also partially explain the larger spread seen with the optical imaging method that is characterized by a low temporal resolution making it inevitable to include later—though also weaker—parts of the responses (Kisvarday et al., 2001).

Interestingly, two types of cortical response profiles were obtained, single- and double peak activity distributions (Fig. 2). We assume that double peaks seen with epi-retinal stimulation might be due to the simultaneous activation of local ganglion cell bodies and passing axons of slightly remote ganglion cells having offset receptive fields (Wilms & Eckhorn, 2005). In this regard, future studies using voltage sensitive dye imaging will be helpful for tracking the spatio-temporal evolution of cortical activity to single vs. multisite activation of the retinal implant.

#### 4.1.1. Influence of electrode size on spatial resolution

The size of the thin-film stimulation electrodes considerably influence the width of the estimate of the cortical activation profile, if their diameter is larger than about 50 μm. At the cat's retinal surface, one millimeter corresponds to about 5° visual angle, i.e., 50 μm is about 0.25° (15′) (in the human eye 1 mm corresponds to approximately 3.4°;

Drasdo & Fowler, 1974). The thin-film electrodes normally used by us had contact points of 100 μm diameter. Thus, a single electrode already covered 0.5° of visual angle and accordingly the spread of retinal and cortical activation covered even larger angles of visual representation. In fact, electrodes giving rise to more localized high current densities like the fiber-cone electrodes with ~20 μm base diameter (Reitböck, 1983) revealed highest resolutions of about 0.7° with epi-retinal stimulation while epi-retinal film electrodes of 100 μm diameter reached only 1.2° (estimated from cortical response distribution; normalized to reference eccentricity of 2°, see Section 2). With sub-retinal stimulation (film electrodes, rectangular electrode areas 100 × 100 μm) similar resolutions were obtained (0.9° to 1.3°; see Table 1).

#### 4.1.2. Influence of recorded signal type

In electrical recordings by microelectrodes, the width of the cortical activation depends on the spatial recording characteristics ("seeing" ranges) of the electrodes and the particular properties of the recorded neural signals, which are different for different signal types. The spatial spread of multiple unit activity (MUA) is in the range of 40 μm in the upper layers of area 17 of the cat (Gray, Maldonado, Wilson, & McNaughton, 1995) and of local field potentials (LFP) about 400 μm (measured with current injection and recording by a linear array of microelectrodes by the authors of the Neurophysics group, University of Marburg). Both values are cortical distances for half height decline. For the smallest measured width of cortical activations (around 1 mm here) this means that we potentially overestimated values based on MUA by about 8% and those with LFP by 80%. However, these influences must be considered in conjunction with the effective lateral coupling width of the neural network involved in the stimulus evoked responses and with the size and form of the stimulation electrodes.

The recording technique of optical imaging captures averaged signals from the cortical surface down to a depth of approximately 700 μm. The recorded intrinsic signals are mainly based on the oxygen consumption and the related deoxygenation of hemoglobin in active cortical regions (for review, see Grinvald et al., 1999); their spatial resolution is influenced by the intercapillary distances in the brain (approximately 50 μm in the cat visual cortex). Inhibitory and excitatory post-synaptic potentials as well as spike responses contribute to the intrinsic signals. Thus, they represent above threshold spike responses and all subthreshold synaptic activity, which all contribute to the width of the distribution of intrinsic signal changes evoked by retinal stimulation.

#### 4.1.3. Influence of lateral connectivities

Our estimate of the spatial resolution on the basis of the cortical activation width may also depend on the effective lateral couplings among evoked signals in the retina, geniculate nucleus, and cortex, which are due to the lateral connectivities in these structures. They include divergent excitatory feed forward connections, of which magno cellular geniculate neurons are particularly broadly projecting to the cortex (Freund, Martin, Soltesz, Somogyi, & Whiteridge, 1989; Humphrey, Saul, & Feidler, 1998) and lateral intracortical facilitatory and disinhibitory connections (Kisvarday & Eysel, 1992). The superimposed influences of all these connectivity-based lateral spreads of activation are about 2–3 mm in the cat primary visual cortex (half height decline measured by signal correlations; Brosch, Bauer, & Eckhorn, 1991). Hence, these widths are equal or even larger than the highest resolutions given in our present report. This is due to the fact that we could take the early cortical response components (from the electrical recordings) which are locally confined, whereas the lateral spread of the activation increases considerably about 20 ms after stimulation (Fig. 1A).

The estimated minimal requirements of spatial resolution for useful artificial vision, investigated by psychophysical methods can be compared and combined with our physiological estimates of achievable spatial resolution under optimal conditions. Reading at central retinal projection sites requires about 300 pixels (20 × 15) within about 5° retinal eccentricity (Sommerhalder et al., 2003). If we take a physiologically achievable resolution of 0.75° and substitute each image pixel by a stimulation electrode with constant spacing, the stimulation array will cover 3.9 by 2.8 $mm^2$ retina (~7.1° by ~5.3° visual eccentricity). If safe navigation in dynamic out-door environments is required, stimulation should include eccentricities of at least 15° (Cha, Horch, Normann, & Boman, 1992b; Geruschat et al., 1998). Since the spatial resolution required for safe navigational purposes outside the reading area can be chosen much coarser (at about 2° electrode pitch) this would add about another 200 electrodes for the outer "navigational belt." Hence, as a minimal condition a total of about 500 well functioning electrodes with comparable stimulation capabilities would be required for an implant usefully spanning a retinal stimulation area of about 8 mm in diameter.

### 4.2. Temporal resolution

The rate of possible temporal modulation can coarsely be estimated from the duration of cortical responses to single electrical impulses applied in the retina. With stimulus currents twice the threshold we measured response durations of about 40 ms at one second stimulus repetitions. However, with higher stimulation rates of 10–50 impulses per second mimicking more natural interval distributions (Gamma), response durations decreased considerably (to 20–30 ms, estimated from the stimulus–response cross-correlations). This corresponds to an increase in temporal resolution which can be caused by several factors such as an increase in the average level of cortical inhibition that keeps the late response phases subthreshold. In addition, higher stimulation rates lead to increased average activations of both excitatory and inhibitory synapses which, in turn, reduce the time constants and increase the frequency

bandwidths of dendrites and somata of ortical neurons (Agmon-Snir & Segev, 1993; Nelson, 1994). Hence, near physiological patterns and high rates of retinal stimulation can result in cortical response durations which are able to code 30–50 temporal changes of two-level intensities per second. However, the pilot experiments of Humayun et al. (1999) with electrical stimulation in human patients suggest somewhat lower frequencies. They created non-flickering perception with rhythmic stimulation already at frequencies between 40 and 50 Hz. Nonetheless, fast temporal changes may be also perceiveable with non-rhythmic (stochastic) stimulation patterns generating non-rhythmic spike patterns in ganglion cells similar to visual responses.

#### *4.2.1. Discrimination among somal and axonal stimulations*

We found that epi-retinal stimulation has to deal with the problem of activation of ganglion cell somata in the vicinity of the electrode tip and of passing axons originating from remote ganglion cell bodies (results not shown here). This problem cannot be neglected, since a simultaneous activation of ganglion cell bodies in the vicinity of the electrode and passing axons may lead to multisite or ambiguous phosphenes (Wilms & Eckhorn, 2005). For a solution of this problem further investigations are required. Cone electrodes protruding to ganglion cell somata through the internal limitating membrane could selectively activate the cell bodies. For selective fiber stimulation, electrode pairs with tips aligned parallel to the fibers and specific stimulation current/time patterns might provide a solution. Finally, offsets of single focal phosphenes due to activation of passing fibers by epi-retinal electrodes can be compensated by an adaptable retina-processor outside of the eye (Eckmiller, 1997). On the other hand, sub-retinal stimulation at retinal eccentricities smaller than 8° would have to face systematic and increasing mislocation of phosphenes with decreasing eccentricity due to the displacement of bipolar and retinal ganglion cells in the central retinal region (Sjöstrand, Olsson, Popovic, & Conradi, 1999). However, the physiological resolution providing a visual acuity of 0.1–0.2 at the desired location of 8° eccentricity corresponds well with the spatial characteristics of sub-retinal chips.

## 5. Conclusions

We obtained relatively high spatial and temporal resolutions of 0.7–1.3° visual angle and 30–40 ms, respectively, with both epi- and sub-retinal stimulation. Spatial resolution can

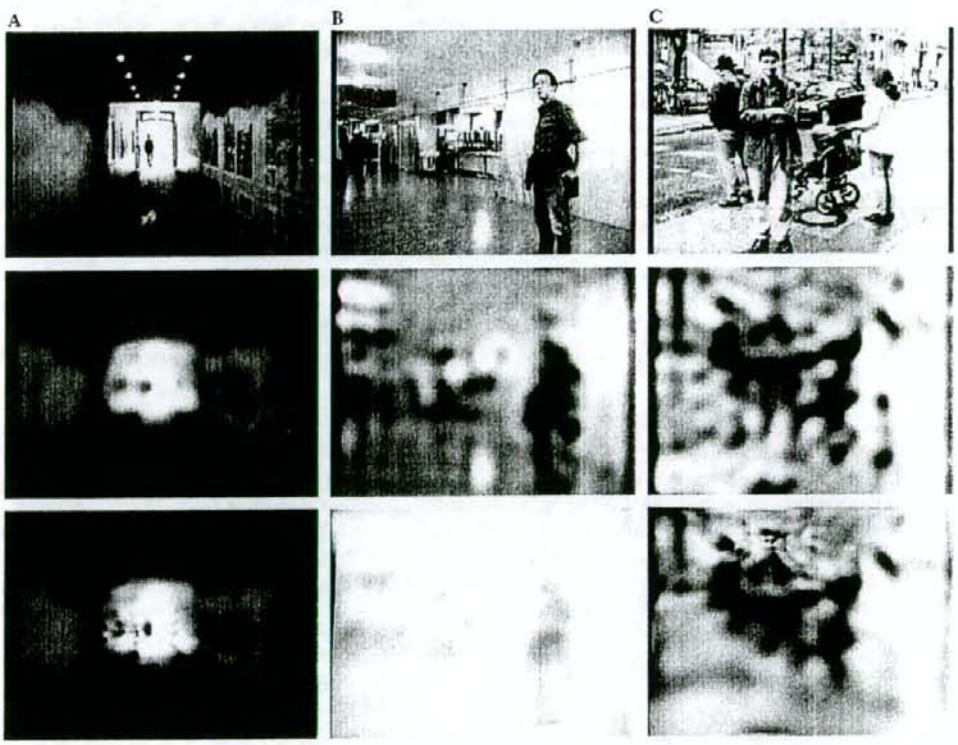


Fig. 6. Real scenes filtered with resolutions obtained in this investigation. (A) Person at the end of a tunnel; (B) person standing in a hall; (C) group of persons on a street. (a) Unfiltered; (b) resampled on a regular cartesian raster; (c) resampled on a irregular hexagonal grid with spatial frequency increasing from periphery to center. Highest resolution is centered on the person at the end of the tunnel (A), head of person (B and C). Gaussian filter kernels at 500 grid positions, simulating Gaussian shaped phosphenes evoked by 500 stimulation electrodes. The output images are restricted to 8 gray tones.

probably be increased up to 0.5° visual angle by choosing smaller-area flat or cone tip electrodes made from materials with higher charge transfer capacity. The highest resolution estimates were reported for electrical stimulation in isolated retinae (Stett et al., 2000) which may be 0.3° visual angle. The upper limit obtained for temporal resolution can further be increased by using higher stimulation rates, mimicking physiological spike patterns of retinal ganglion cells. Since the resolutions reported here were estimated from cortical recordings, direct relations to visual perception are possible, including the expected perception by the blind patients, but may underestimate the finally achievable resolution. We assume that the resolutions obtainable with electronic retinal implants are sufficient for visuo-motor coordination in many in- and out-door situations of daily life. We demonstrate this by movie presentations of simulated perceptions (example clips in Fig. 6) obtained by filtering typical visual scenes with the resolution values obtained in this investigation (accessible under http://neuro.physik.uni-marburg.de/~retina-implant/). Our results indicate that spatial resolution achieved by sub- or epi-retinal stimulation should be sufficient to gain useful object recognition in dynamic environments.

## Acknowledgments

The authors acknowledge the cooperation of many colleagues involved in the project (for the presentation of the consortium, see www.uni-tuebingen.de/rim and www.nero.uni-bonn.de and www.neuro.physik.uni-marburg.de/~retina-implant). We also are very grateful for the support by the German Ministry of Research and Technology (01KP0007, 01KP0008) and for the Support by Pro Retina Deutschland e.V. and the Ewald und Karin Hochbaum-Foundation.

## References

Adams, D. L., & Horton, J. C. (2003). A precise retinotopic map of primate striate cortex generated from the representation of angioscotomas. *Journal of Neuroscience, 23*, 3771–3789.

Agmon-Snir, H., & Segev, I. (1993). Signal delay and input synchronization in passive dendritic structures. *Journal of Neurophysiology, 70*, 2066–2085.

Angelucci, A., Levitt, J. B., Walton, E. J. S., Hupé, J.-M., & Bullier, J. (2002). Circuits for local and global signal integration in primary visual cortex. *Journal of Neuroscience, 22*, 8633–8646.

Bonhoeffer, T., & Grinvald, A. (1996). Optical imaging based on intrinsic signals. The methodology. In A. W. Toga & J. C. Mazziotta (Eds.), *Brain mapping: The methods* (pp. 55–97). San Diego: Academic Press.

Brosch, M., Bauer, R., Eckhorn, R. (1991). Spatial correlation profiles of stimulus-induced oscillatory activities in cat visual cortex. *Proceedings of the Goettingen Neurobiology Conference*, New York: Thieme, p 214.

Bullier, J., Hupe, J.-M., James, A. C., & Girard, P. (2001). The role of feedback connections in shaping the responses of visual cortical neurons. *Progress in Brain Research, 134*, 193–204.

Cha, K., Horch, K. W., & Normann, R. A. (1992a). Mobility performance with a pixelized vision system. *Vision Research, 32*, 1367–1372.

Cha, K., Horch, K. W., Normann, R. A., & Boman, D. (1992b). Reading speed with a pixelized vision system. *Journal of the Optical Society of America A. 9*, 673–677.

Chow, A. Y., & Chow, V. Y. (1997). Subretinal electrical stimulation of the rabbit retina. *Neuroscience Letters, 225*, 13–16.

Chow, A. Y., Pardue, M. T., Chow, V. Y., Peyman, G. A., Liang, C., Perlman, J. I., et al. (2001). Implantation of silicon chip microphotodiode arrays into the cat subretinal space. *IEEE Transactions on Neural Systems and Rehabilitation Engineering, 9*, 86–95.

Chow, A. Y., Pardue, M. T., Perlman, J. I., Ball, S. L., Chow, V. Y., Hetling, J. R., et al. (2002). Subretinal implantation of semiconductor-based photodiodes: Durability of novel implant designs. *Journal of Rehabilitation Research and Development, 39*, 313–321.

Darian-Smith, C., & Gilbert, C. D. (1995). Topographic reorganization in the striate cortex of the adult cat and monkey is cortically mediated. *Journal of Neuroscience, 15*, 1631–1647.

Dinse, H., & Krüger, K. (1994). The timing of processing along the visual pathway in the cat. *Neuroreport, 5*, 893–897.

Drasdo, N., & Fowler, C. W. (1974). Non-linear projection of the retinal image in a wide angle schematic eye. *British Journal of Ophthalmology, 58*, 709–714.

Eckhorn, R., & Pöpel, B. (1975). Rigorous and extended application of information theory to the afferent visual system of the cat. II. Experimental results. *Biological Cybernetics, 17*, 7–17.

Eckhorn, R., Grüsser, O.-J., Kröller, J., Pellnitz, K., & Pöpel, B. (1976). Efficiency of different neural codes: Information transfer calculations for three different neuronal systems. *Biological Cybernetics, 32*, 243–248.

Eckhorn, R., & Pöpel, B. (1981). Responses of cat retinal ganglion cells to the random motion of a spot stimulus. *Vision Research, 21*, 435–443.

Eckhorn, R., Frien, A., Bauer, R., Woelbern, T., & Kehr, H. (1993). High frequency (60–90 Hz) oscillations in primary visual cortex of awake monkey. *Neuroreport, 4*, 243–246.

Eckhorn, R., & Thomas, U. (1993). A new method for the insertion of multiple microprobes into neural and muscular tissue, including fiber electrodes, fine wires, needles and microsensors. *Journal of Neuroscience Methods, 49*, 175–179.

Eckmiller, R. (1997). Learning retina implants with epiretinal contacts. *Ophthalmic Research, 29*, 281–289.

Eger, M., Wilms, M., Eckhorn, R., & Schanze, T. (2005). Information transmission from a retina implant to the cat visual cortex. *Biosystems, 79*, 133–142.

Eysel, U. T., Grüsser, O.-J., & Pecci Saavedra, J. (1974). Signal transmission through degenerating synapses in the lateral geniculate body of the cat. *Brain Research, 76*, 49–70.

Freund, T. F., Martin, K. A. C., Soltesz, I., Somogyi, P., & Whiteridge, D. (1989). Arborisation pattern and postsynaptic targets of physiologically identified thalamocortical afferents in striate cortex of the macaque monkey. *Journal of Comparative Neurology, 289*, 315–336.

Gail, A., Brinksmeyer, H. J., & Eckhorn, R. (2000). Contour decouples gamma activity across texture representation in monkey striate cortex. *Cerebral Cortex, 10*, 840–850.

Gekeler, F., Kobuch, K., Schwahn, H. N., Stett, A., Shinoda, K., & Zrenner, E. (2004). Subretinal electrical stimulation of the rabbit retina with acutely implanted electrode arrays. *Graefes Archiv of Clinical and Experimental Ophthalmology, 242*, 587–596.

Geruschat, D. R., Turano, K. A., & Stahl, J. W. (1998). Traditional measures of mobility performance and retinitis pigmentosa. *Optometry and Visual Sciences, 75*, 525–537.

Gilbert, C. D., & Wiesel, T. N. (1990). The influence of contextual stimuli on the orientation selectivity of cells in primary visual cortex of the cat. *Vision Research, 30*, 1689–1701.

Gilbert, C. D. (1993). Circuitry, architecture, and functional dynamics of visual cortex. *Cerebral Cortex, 3*, 373–386.

Gray, C. M., Maldonado, P. E., Wilson, M., & McNaughton, B. (1995). Tetrodes markedly improve the reliability and yield of multiple single-unit isolation from multi-unit recordings in cat striate cortex. *Journal of Neuroscience Methods, 63*, 43–54.

Grind van de, W. A., Grüsser, O. J., & Lunkenheimer, H. U. (1973). Perception and physiology of flicker vision. In *Central processing of visual information. A: Integrative functions and comparative data, handbook of sensory physiology* (Vol. VII/3). Berlin, New York: Springer.

Grinvald, A., Lieke, E., Frostig, R., & Hildesheim, R. (1994). Cortical point spread function and long-range lateral interactions revealed by real-time optical imaging of macaque monkey primary visual cortex. *Journal of Neuroscience, 14*, 2545–2568.

Grinvald, A. D., Shoham, A., Shmuel, D. E., Glaser, I., Vanzetta, E., Shtoyerman, H., et al. (1999). In-vivo optical imaging of cortical architecture and dynamics. A. In U. Windhorst & H. Johansson (Eds.), Modern techniques in neuroscience research. Springer, pp. 893–969.

Grüsser, O.-J., & Creutzfeld, O. (1957). Eine neurophysiologische Grundlage des Brücke-Bartley-Effektes: Maxima der Impulsfrequenz retinaler und corticaler Neurone bei Flimmer-Licht mittlerer Frequenzen. *Pflügers Archiv der gesamten Physiologie, 263*, 668–681.

Hesse, L., Schanze, T., Wilms, M., & Eger, M. (2000). Implantation of retina stimulation electrodes and recording of electrical stimulation responses in the visual cortex of the cat. *Graefe's Archiv of Clinical and Experimental Ophthalmology, 238*, 840–845.

Heydt von der, R., & Peterhans, E. (1989). Mechanisms of contour perception in monkey visual cortex. I. Lines of pattern discontinuity. *Journal of Neuroscience, 9*, 1731–1748.

Hubel, D., & Wiesel, T. (1962). Receptive fields, binocular interaction, and functional architecture in the cat's visual cortex. *Journal of Physiology, 160*, 106–154.

Humayun, M. S., Probst, R. H., Juan, E. de., McCormick, K., & Hickingbotham, D. (1994). Bipolar surface electrical stimulation of the vertebrate retina. *Archive of Ophthalmology, 112*, 110–116.

Humayun, M. S., Juan, E. de., Dagnelie, G., Greenberg, R. J., Probst, R. H., & Phillips, D. H. (1996). Visual perception elicited by electrical stimulation of retina in blind humans. *Archive of Ophthalmology, 114*, 40–46.

Humayun, M. S., Juan, E. de., Weiland, J. D., Dagnelie, G., Katona, S., Greenberg, R., et al. (1999). Pattern electrical stimulation of the human retina. *Vision Research, 39*, 2569–2576.

Humayun, M. S., Weiland, J. D., Fujii, G. Y., Greenberg, R., Williamson, R., Little, J., et al. (2003). Visual perception in a blind subject with a chronic microelectrode retinal prosthesis. *Vision Research, 43*, 2573–2581.

Humphrey, A. L., Saul, A. B., & Feidler, J. C. (1998). Strobe rearing prevents the convergence of inputs with different timings onto area 17 simple cells. *Journal of Neurophysiology, 80*, 3005–3020.

Kisvarday, Z. F., Buzas, P., & Eysel, U. T. (2001). Calculating direction maps from intrinsic signals revealed by optical imaging. *Cerebral Cortex, 11*, 636–647.

Kisvarday, Z. F., & Eysel, U. T. (1992). Cellular organization of reciprocal patchy networks in layer III of cat visual cortex (area 17). *Neuroscience, 46*, 275–286.

Knierim, J. J., & van Essen, D. C. (1992). Neuronal responses to static texture patterns in area V1 of the alert macaque monkey. *Journal of Neurophysiology, 67*, 961–980.

Lamme, V. A. F., Rodriguez-Rodriguez, V., & Spekreijse, H. (1999). Separate processing dynamics for texture elements, boundaries and surfaces in primary visual cortex of the macaque monkey. *Cerebral Cortex, 9*, 406–413.

Legge, G. E., Ahn, S. J., Klitz, T. S., & Luebker, A. (1997). The visual span in normal and low vision. *Vision Research, 37*, 1999–2010.

Mitzdorf, U. (1987). Properties of the evoked potential generators: Current source-density analysis of visually evoked potentials in cat cortex. *The Journal of Neuroscience, 33*, 33–59.

Nelson, M. E. (1994). A mechanism for neuronal gain control by descending pathways. *Neural Computation, 6*, 242–254.

Nirenberg, S., Carcieri, S. M., Jacobs, A. L., & Latham, P. E. (2001). Retinal ganglion cells act largely as independent encoders. *Nature, 411*, 698–701.

Normann, R. A., Maynard, E. M., Guillory, K., & Warren, D. J. (1996). Cortical implants for the blind. *IEEE Spectrum, 33*, 54–59.

Normann, R. A., Maynard, E. M., Rousche, P. J., & Warren, D. J. (1999). A neural interface for a cortical vision prosthesis. *Vision Research, 39*, 2577–2587.

Orban, G. A. (1984). *Neuronal operations in the visual cortex*. Berlin, New York: Springer.

Peyman, G., Chow, A. Y., Liang, C., Chow, V. C., Perlman, J. I., & Peachey, N. S. (1998). Subretinal semiconductor microelectrode array. *Ophthalmic Surgery and Lasers, 29*, 234–241.

Rager, G., & Singer, W. (1998). The response of cat visual cortex to flicker stimuli of variable frequency. *European Journal of Neuroscience, 10*, 1856–1877.

Ratzlaff, E. H., & Grinvald, A. (1991). A tandem-lens epifluorescence macroscope: Hundred-fold brightness advantage for wide-field imaging. *Neuroscience Methods, 36*, 127–137.

Reitböck, H. J. (1983). Fiber microelectrodes for electrophysiological recordings. *Journal of Neuroscience Methods, 8*, 249–262.

Rieke, F., Warland, D. K., de Ruyter van Steveninck, R. R., & Bialek, W. (1998). *Spikes: Exploring the neural code*. Cambridge: MIT Press.

Rizzo, J. F., Loewenstein, J., Kelly, S., Shire, D., Herndon, T., & Wyatt, J. L. (1999). Electrical stimulation of human retina with a microfabricated electrode array. *Investigative Ophthalmology and Visual Science, 40*, S783.

Rizzo, J. F., & Wyatt, J. L. (1997). Prospects for a visual prosthesis. *The Neuroscientist, 3*, 251.

Sachs, H. G., Kobuch, K., Miliczek, K. D., Kohler, K., Zrenner, E., & Gabel, V.-P. (1999). The Yucatan micropig model for implantation of subretinal microphotodiode arrays (MPDA) in visual prosthetic research. *Investigative Ophthalmology and Visual Sciences, 40*, S734.

Salzman, C. D., Britten, K. H., & Newsome, W. T. (1990). Cortical microstimulation influences perceptual judgements of motion direction. *Nature, 346*, 174–177.

Santos, A., Humayun, M., de Juan, E., Greenburg, R. J., Marsh, M., Klock, I., et al. (1997). Preservation of the inner retina in retinitis pigmentosa. *Archive of Ophthalmology, 115*, 511–515.

Schanze, T., Wilms, M., Eger, M., Hesse, L., & Eckhorn, R. (2002). Activation zones in cat visual cortex evoked by electrical retina stimulation. *Graefe's Archiv of Clinical and Experimental Ophthalmology, 240*, 947–954.

Schwahn, H. N., Gekeler, F., Kohler, K., Kobuch, K., Sachs, H. G., Schulmeyer, F., et al. (2001). Studies on the feasibility of a subretinal visual prosthesis: Data from Yucatan micropig and rabbit. *Graefes Archive of Clinical and Experimental Ophthalmology, 239*, 961–967.

Seiler, M. J., Aramant, R. B., & Ball, S. L. (1999). Photoreceptor function of retinal transplants implicated by light–dark shift of s-antigen and rod transducin. *Vision Research, 39*, 2589–2596.

Shannon, C. E. (1948). A mathematical theory of communication. *Bell Systems Technical Journal, 27*, 623–656.

Shapley, R. M., & Victor, J. D. (1981). How the contrast gain control modifies the frequency responses of cat retinal ganglion cells. *Journal of Physiology, 318*, 161–179.

Shevelev, I. A., Eysel, U. T., Lazareva, N. A., & Sharaev, G. A. (1998). The contribution of intracortical inhibition to dynamics of orientation tuning in cat striate cortex neurons. *Neuroscience, 84*, 11–23.

Sjöstrand, J., Olsson, V., Popovic, Z., & Conradi, N. (1999). Quantitative estimations of foveal and extra-foveal retinal circuitry in humans. *Vision Research, 39*, 2987–2998.

Sommerhalder, J., Oueghlani, E., Bagnoud, M., Leonards, U., Safran, A., & Pellizone, M. (2003). Simulation of artificial vision: I. Eccentric reading of isolated words, and perceptual learning. *Vision Research, 43*, 269–283.

Stett, A., Barth, W., Weiss, S., Haemmerle, H., & Zrenner, E. (2000). Electrical multisite stimulation of the isolated chicken retina. *Vision Research, 40*, 1785–1795.

Stieglitz, T., Beutel, H., Schuettler, M., & Meyer, J. (2000). Micromachined polyimide-based devices for flexible neural interfaces. *Biomedical Microdevices, 2*, 283–294.

Sutter, E. E. (2001). Imaging visual function with the multifocal m-sequence technique. *Vision Research, 41*, 1241–1255.

Tovee, M. J. (1996). *An introduction to the visual system*. Cambridge University Press.

Tusa, R. J., Palmer, L. A., & Rosenquist, A. C. (1978). The retinotopic organization of area 17 (striate cortex) in the cat. *Journal of Comparative Neurology, 177*, 213–236.

Tusa, R. J., Rosenquist, A. C., & Palmer, L. A. (1979). Retinotopic organization of areas 18 and 19 in the cat. *Journal of Comparative Neurology, 185*, 657–678.

Volker, M., Shinoda, K., Sachs, H., Gmeiner, H., Schwarz, T., Kohler, K., et al. (2006). In vivo assessment of subretinally implanted microphotodiode arrays in cats by optical coherence tomography and fluorescein angiography. *Graefes Archiv of Clinical and Experimental Ophthalmology*, (in press).

Wachtler, T., Sejnowski, T. J., & Albright, T. D. (2003). Representation of color stimuli in awake macaque primary visual cortex. *Neuron, 37*, 681–691.

Waessle, H., & Boycott, B. B. (1991). Functional architecture of the mammalian retina. *Physiological Reviews, 71*, 447–480.

Wilms, M., Eger, M., Schanze, T., & Eckhorn, R. (2003). Visual resolution with epi-retinal electrical stimulation estimated from activation profiles in cat visual cortex. *Visual Neuroscience, 20*, 543–555.

Wilms, M., & Eckhorn, R. (2005). Spatiotemporal receptive field properties of epiretinally recorded spikes and local electroretinograms in cats. *BMC Neuroscience, 6*, 50.

Wyatt, J., & Rizzo, J. (1996). Ocular implants for the blind. *IEEE Spectrum, 33*, 47–53.

Xu, X.-M., Ichida, J., Allison, J. D., Bonds, A. B., & Casagrande, V. A. (2001). A comparison of koniocellular, magnocellular and parvocellular receptive field properties in the lateral geniculate nucleus of thed owl monkey (aotus trivirgatus). *Journal of Physiology (Lond.), 531*, 203–218.

Zrenner, E., Miliczek, K. D., Gabel, V., Graf, H., Guenther, E., Haemmerle, H., et al. (1997). The development of subretinal microphotodiodes for replacement of degenerated photoreceptors. *Ophthalmic Research, 29*, 269–280.

Zrenner, E., Stett, A., Weiss, S., Aramant, R. B., Guenther, E., Kohler, K., et al. (1999). Can subretinal microphotidiodes successfully replace degenerated photoreceptors? *Vision Research, 39*, 2555–2567.

Zrenner, E. (2002). Will retinal implants restore vision? *Science, 295*, 1022–1025.

Available online at www.sciencedirect.com
SCIENCE DIRECT
Experimental Eye Research 83 (2006) 329–338
EXPERIMENTAL EYE RESEARCH
www.elsevier.com/locate/yexer

# Expression of endostatin in human choroidal neovascular membranes secondary to age-related macular degeneration

Olcay Tatar [a], Kei Shinoda [b], Annemarie Adam [c], Jens Martin Rohrbach [a], Klaus Lucke [d], Sigrid Henke-Fahle [a], Karl Ulrich Bartz-Schmidt [a], Salvatore Grisanti [a,*]

[a] *University Eye Clinic at the Centre for Ophthalmology of the Eberhard-Karls-University Tübingen, Schleichstrasse 12-15, 72076 Tuebingen, Germany*
[b] *Laboratory of Visual Physiology, National Institute of Sensory Organs, National Hospital Organization, Tokyo Medical Center, Japan*
[c] *Department of Pathology, Eberhard-Karls-University, Tuebingen, Germany*
[d] *Eye Clinic Universitätsallee, Bremen, Germany*

Received 7 June 2005; accepted in revised form 21 December 2005
Available online 11 April 2006

**Abstract**

Endostatin is an endogenous angiogenesis inhibitor which requires E-selectin for its antiangiogenic activity. The aim of this study was to investigate the expression of endostatin in human choroidal neovascular membranes (CNV) secondary to age-related macular degeneration (AMD) with regard to vascularization and proliferative activity. An interventional case series of 36 patients who underwent removal of CNV were retrospectively investigated. Thirty-six CNV were analyzed by light microscopic immunohistochemistry for the expression of CD34 (endothelial cells, EC), CD105 (activated EC), Ki-67 (cell proliferation), Cytokeratin 18 (epithelial cells), VEGF (vascular endothelial growth factor), E-selectin and endostatin. Donor eyes ($n = 7$) including one with AMD were used as controls. Endostatin immunoreactivity was present in choroidal vessels of five as well as in the retinal pigment epithelium (RPE)-Bruch's membrane complex of two donor eyes without AMD. In one eye with AMD, endostatin was detected in RPE, Bruch's membrane and choroidal vessels. Ninety-two percent (33/36) of CNV disclosed endostatin staining. RPE-Bruch's membrane complex, choroidal vessels and stroma were positive in 50% (18/36), 72% (26/36), and 78% (28/36) of the membranes, respectively. Both control eyes and CNV expressed all the investigated markers except E-selectin being positive only in membranes. Endostatin, an endogenous angiogenesis inhibitor, is expressed in CNV and its therapeutic up-regulation may be a new strategy in the treatment of neovascular AMD.


*Keywords:* age-related macular degeneration; choroidal neovascularization; angiogenesis; endostatin; E-selectin

## 1. Introduction

Choroidal neovascularization (CNV) is responsible for the majority of severe visual loss due to age-related macular degeneration (AMD), the most common cause of visual morbidity in elderly (The Macular Photocoagulation Study Group, 1991). Recent studies have clarified the importance of a balance between local inhibitory and stimulatory factors in the pathogenesis of angiogenesis (Pepper, 2001), but some of these factors still remain to be defined.

Endostatin, a 20 kDa C-terminal fragment of collagen XVIII, has been identified as an endogenous angiogenesis inhibitor (O'Reilly et al., 1997). Collagen XVIII is the core protein of a heparan sulfate proteoglycan in vascular and epithelial basement membranes (Zatterstrom et al., 2000). Endostatin is bound to collagen XVIII by a protease-sensitive hinge. Some proteases, such as matrix metalloproteases (MMPs), can cleave the hinge so that endostatin can be released and becomes available (Sasaki et al., 1998; Ferreras et al., 2000).

* Corresponding author. Tel.: +49 7071 2984004; fax: +49 7071 295215.
*E-mail address:* salvatore.grisanti@med.uni-tuebingen.de (S. Grisanti).

0014-4835/$ - see front matter © 2006 Elsevier Ltd. All rights reserved.
doi:10.1016/j.exer.2005.12.017

The antiangiogenic effect of endostatin is both at the transcriptional and cellular level. At the transcriptional level, endostatin down-regulates proangiogenic genes related to vascular endothelial growth factor (VEGF) signalling (e.g. thrombin receptors, Stats, and HIF-1), but up-regulates antiangiogenic genes (such as Vasostatin, Kininogen) in human microvascular endothelial cells (EC) (Abdollahi et al., 2004). On the cellular level, endostatin was shown to inhibit EC proliferation and migration stimulated by FGF-2 (Eriksson et al., 2003), EC chemotactic migration towards VEGF (Eriksson et al., 2003; Yamaguchi et al., 1999) and EC invasion by blocking the activation and catalytic activity of MMP-2 (Lee et al., 2002; Kim et al., 2000). Additionally, endostatin induces EC apoptosis (Dhanabal et al., 1999; Dixelius et al., 2000). Lately, E-selectin, a cellular adhesion molecule, was proven to be required for the antiangiogenic activity of endostatin (Yu et al., 2004).

EC in different parts of the body have different characteristics (Lanzer and Raff, 1987). Variations in surrounding cells and extracellular matrix may also contribute to the tissue-specific aspects of neovascularization (Mori et al., 2001). The altered local balance between stimulators and inhibitors is accepted to be the cause of neovascularization (Pepper, 2001; Mori et al., 2001); however, the involved players may vary depending on the setting.

All the aforementioned angiogenic factors (FGF, VEGF, MMP, HIF-1) seem to have well-defined roles in the pathogenesis and development of CNV (Amin et al., 1994; Kvanta et al., 1996; Martin et al., 2004; Lambert et al., 2003). Endostatin, shown to inhibit their activities and known to up-regulate antiangiogenesis genes, therefore, is likely to be an endogenous inhibitor of angiogenesis also in CNV. Intravitreal or intravenous delivery of endostatin by viral vectors was shown to inhibit diabetic retinopathy and choroidal neovascularization in experimental studies (Mori et al., 2001; Auricchio et al., 2002). Bhutto et al. (2004) evaluated endostatin expression in five donor eyes with advanced AMD—four eyes with disciform scar with small CNV and one eye with geographic atrophy with sub-RPE neovascularization—and reported nearly absent endostatin expression. However, to the best of our knowledge, expression of this endogenous angiogenesis inhibitor in active CNV membranes extracted surgically before they reach the disciform scar stage has not been defined experimentally or clinically yet.

The aim of this study was to analyze the endostatin expression in surgically extracted active human CNV with regard to vascularization and proliferative activity. The level of vascularization was determined by the expression of CD 34, a pan-endothelial cell marker, and CD105 (Endoglin), a marker for activated endothelial cells (Grisanti et al., 2004).

Ki-67, Cytokeratin18 (CK18) and an antibody specific for VEGF-A were used to detect the proliferative activity (Grisanti et al., 2004), to identify RPE cells (Martin et al., 2004) and to evaluate the angiogenic stimulation, respectively. Expression of E-selectin which is required for the antiangiogenic activity of endostatin (Yu et al., 2004) was analyzed both in control eyes and CNV.

## 2. Materials and methods

### 2.1. Subjects and treatment

We retrospectively reviewed 36 CNV, secondary to neovascular AMD, from 36 eyes of 36 consecutive patients, in which three-port vitrectomy and extraction of CNV was performed. None of the patients had disciform scar but CNV with submacular leakage or hemorrhage leading to progressive visual deterioration. CNV membranes previously treated with photodynamic therapy, laser coagulation or any kind of anti-angiogenesis therapy including intravitreal triamcinolone injection were not included in our series. Each patient gave written informed consent after the nature of the procedure and alternatives had been fully explained. The study followed the guidelines of the declaration of Helsinki as revised in Tokyo and Venice and adhered to the requirements of the local Institutional Review Board. The histological analysis of the specimens was approved by the Institutional Ethic Committee. Normal donor eyes ($n = 6$) and a donor eye with drusen but without neovascularization ($n = 1$) received for keratoplasty were used as controls.

### 2.2. Tissue preparation

Within minutes after surgery, excised CNV and donor eyes were fixed in 3.7% formalin and subsequently embedded in paraffin. Each specimen was serially sectioned into 5-μm sections and mounted on poly-L-lysine coated glass slides (Dako, Glostrup, Denmark) for immunohistochemical staining. Hematoxylin–eosin and PAS staining were performed to determine the histologic orientation. PAS staining was primarily used to confirm the location of the diffuse drusen and to help the overall orientation of the specimens.

### 2.3. Immunohistology

After serial paraffin sections were de-paraffinized and rehydrated with a graded series of alcohol, different techniques for antigen retrieval were applied. For CK18 and endostatin, antigen retrieval was accomplished by proteolytic digestion with 0.5% protease type XXIV (Bacterial, Sigma, St. Louis, MO) whereas proteinase K (Dako) was used for VEGF. For Ki-67, CD34, CD105 and E-selectin staining, antigen retrieval was accomplished with heat treatment in citrate buffer in a pressure cooker for 2 min.

Immunohistochemical staining for CD105, CD34, Ki-67, CK18 and E-selectin was performed using the horseradish peroxidase method according to the manufacturer's protocol (Vectastain Universal Elite ABC PK-6200 kit, Vector Laboratories, Burlinghame, CA). To block endogenous peroxidase activities, 3% hydrogen peroxide and 0.1% sodium acid were applied to each section. Subsequently, the sections were incubated with horse serum (30 min). Thereafter, specimens were incubated with the primary antibodies specific for human CD105 (mouse, Mab, Clone SN6h, Dako), CD34 (mouse, Mab, Immunotech, Hamburg, Germany), Ki-67

(mouse, Mab, Clone Ki-S5, Dako), and CK 18 (mouse, Mab, Progen, Heidelberg, Germany) and E-selectin (mouse, Mab, Novocastra, UK) for 1 h at room temperature. After incubating with the biotinylated horse anti-mouse anti-rabbit secondary antibody and the ABC Complex (Vectastain Universal Elite ABC PK-6200 kit, Vector Laboratories) for 15 min, followed by washing in-between and afterwards, the antibody-treated sections were developed with a 3-diaminobenzidine (Fluka, Buchs, Germany) solution combined with $H_2O_2$ for CD34, CD105 and Ki-67 staining. For CK 18 and E-selectin staining, the chromogen was replaced with AEC high sensitive substrate chromogen (Cytomation, Code K3461, Dako).

Immunohistochemical stainings for VEGF and endostatin were performed by the alkaline-phosphatase method according to the manufacturer's instructions (ChemMate Detection Kit, Alkaline Phosphatase/RED, Rabbit/Mouse, K5005; Dako). Briefly, after proteolytic digestion with proteinase K (Dako) for 10 min, the sections were incubated with the anti-VEGF primary antibody (mouse, Mab, clone C-1; Santa Cruz Biotechnology, Santa Cruz, CA) for 2 h at 37 °C. For endostatin immunostaining, following proteolytic digestion with protease (Protease XXIV, Sigma) for 10 min, the sections were incubated with the primary endostatin antibody (rabbit, polyclonal, Dianova GmbH, Hamburg, Germany) for 1 h at 37 °C. They were subsequently incubated with the linking biotinylated goat anti-mouse anti-rabbit secondary antibody (ChemMate Link, Biotinylated Secondary Antibodies, AB2, Dako), and with the streptavidin conjugated to alkaline phosphatase for 30 min each. Chromogen Red (ChemMate Detection Kit, Dako) was used as a chromogenic substrate. Levamisole was applied to inhibit endogenous alkaline phosphatase activity. Hematoxylin III according to Gill (Merck, Darmstadt, Germany) was used as a counterstain. For negative controls, the primary antibodies were substituted either by appropriate normal sera or omitted.

For better visualization of positive areas, donor eyes and CNV were examined after melanin bleaching. Melanin bleaching was performed according to the protocol established by Kivela (1995) and Makitie et al. (1998).

### 2.4. Analysis

Slides were analyzed by light microscopy. Intensity and presence of staining were determined three times independently by two masked observers (OT, SG) and the median score for each specimen was obtained. Inter- and intra-observer agreement was found in about 98% of the cases.

Based on the previous studies (Kvanta et al., 1996; Grossniklaus et al., 2002), the CNV membranes were classified as "inflammatory active (IA)" when inflammatory cells were more dominant than fibrosis (i.e. >50% inflammatory cells) or "inflammatory inactive (II)" when fibrosis was more dominant (<50% inflammatory cells) with minor or absent inflammatory response in CNV membranes.

Vascularization was evaluated by analyzing the specimens stained for CD34 and CD105 and counting the numbers of stained vessels in the most vascularized area under ×200 magnification. Every positive-staining endothelial cell or cell cluster that was separate from other vessels was counted irrespective of the staining intensity or the presence of a vascular lumen.

All Ki-67 positive nuclei in RPE, EC and stromal cells were counted separately in each specimen. The percentages of the Ki-67 expressing RPE, EC and stromal cells with regard to the total number of proliferating cells were determined. Proliferative activity (nuclei/mm$^2$) of a membrane was defined as the number of Ki-67 expressing nuclei in 1 mm$^2$ area of a specimen. Proliferative activity in each specimen was determined quantitatively by calculating the ratio of the total number of Ki-67 positive nuclei in CNV to the area of the membrane (mm$^2$).

Immunoreactivity for VEGF, endostatin and E-selectin was analyzed separately in RPE-Bruch's membrane complex, vessels and stroma. A grading scheme indicating the degree of staining was used. The values 3, 2, 1, 0 were assigned to indicate intense (70–100% positive cells), moderate (40–69% positive cells), weak labelling (1– 39% positive cells) and absence (–) of any staining, respectively. An "endostatin overall staining score", "E-selectin overall staining score" and "VEGF overall staining score" (range 0–9) was assigned to each membrane by summing up the staining scores in the three structures (RPE, stroma, EC) evaluated separately.

Statistics for the evaluation of proliferative activity and staining scores in the defined subgroups was performed with Mann–Whitney $U$ test due to high variability of specimens. For correlation analysis, Spearman's correlation test was used; $p \leq 0.05$ was considered significant.

## 3. Results

### 3.1. Histologic characterization of control eyes

Six of the donor eyes ($n = 7$) were normal eyes without any ocular pathology, especially those associated with angiogenesis. One of the seven control eyes, however, disclosed drusen and sub-RPE deposits but no neovascularization. Demographic features and the immunohistologic findings of the control eyes are shown in Table 1 and Fig. 1, respectively.

For a better visualization and evaluation of the immunoreactivity within the choroid-Bruch's membrane-RPE complex, the melanin pigment was bleached. The staining pattern did not change after bleaching. Choroidal vessels displayed endostatin in 5 of 6 normal control eyes (Fig. 1A). Most of the choroidal vessels were endostatin positive in four of these

Table 1
Demographic features of the control eyes

| Control eye | Age, sex | Eye | AMD |
|---|---|---|---|
| 1 | 39, f | Right | – |
| 2 | 62, m | Right | – |
| 3 | 43, m | Right | – |
| 4 | 52, f | Left | – |
| 5 | 39, f | Left | – |
| 6 | 49, f | Left | – |
| 7 | 59, f | Right | + |

AMD, age-related macular degeneration; f, female; m, male.

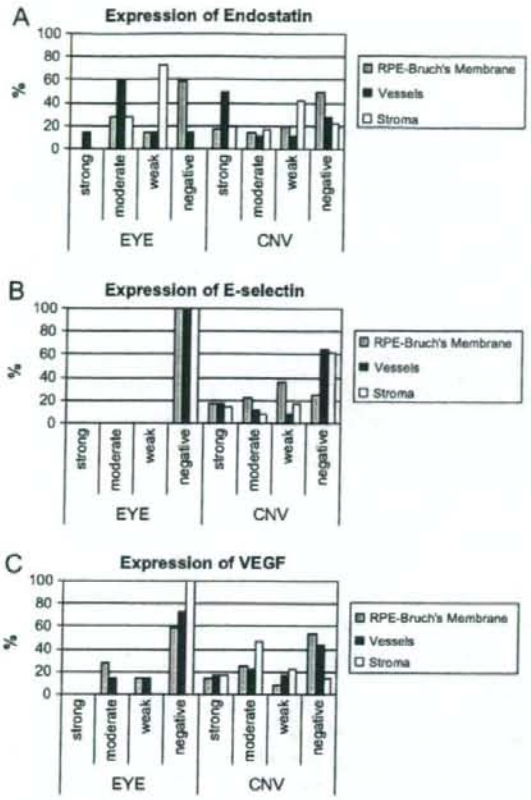


Fig. 1. Immunohistopathologic characteristics of the control eyes and CNV by analysis of the specimens for endostatin (A), E-selectin (B), and VEGF (C) separately in RPE-Bruch's membrane complex, vessels and stroma. For semi-quantitative evaluation, a grading scheme was used indicating the degree of staining: "strong" (70–100% positive cells); "moderate" (40–69% positive cells); "weak" (1–39% positive cells), "negative" (no positive cells).

eyes whereas in one eye only a few of the vessels expressed endostatin (Fig. 2A). The negative control of the same specimen by omitting the primary endostatin antibody displayed no staining in any of the structures (Fig. 2B). Endostatin staining was not specific to vessels. In 2 of 6 control eyes, RPE cells and Bruch's membrane were also stained for endostatin (Figs. 1A and 2C). Endostatin was not diffusely stained throughout a specimen as some endostatin expressing vessels (Fig. 2A) and RPE-Bruch's membrane complex (Fig. 2C) are detected beside the endostatin negative ones in the same specimen (Fig. 2A,D). Endostatin expression and variability in its pattern may be due to the local activity of the proteases in the setting which cleave only some of the endostatin from collagen XVIII. The absence of endostatin expression in RPE-Bruch's membrane complex in four of the control donor eyes (age range 39–62) leads us to assume that this commercial endostatin antibody detects only the free (cleaved) but not the bound form of endostatin. Staining for endostatin in varying intensities was seen in the choroidal stroma of all eyes. In the eye with drusen, endostatin expression was found in RPE-Bruch's membrane complex, stroma and choroidal vessels.

We next sought to investigate the expression of E-selectin and VEGF in the choroid. We found that none of the control eyes displayed E-selectin at all (Figs. 1B and 2E). In contrast, VEGF expression was present but still weak. RPE cells expressed VEGF moderately in two of the eyes. Weak to moderate expression of VEGF in choroidal vessels was also detected only in two eyes (Figs. 1C and 2F).

### 3.2. Histologic characterization of the CNV

All but one CNV were vascularized as evidenced by CD34 positive vessels. CD105 staining was specific to EC (Fig. 3A). CD105 was expressed in all the vascularized specimens ($n = 35$) to some extent (Fig. 3A). Within 13 of 35 vascularized CNV membranes (37%), some vascular ECs positive for CD34 did not express CD105. Contrary to control eyes, E-selectin was detected in RPE-Bruch's membrane, EC and some stromal cells in 75%, 36%, and 39% of CNV, respectively (Figs. 1B and 3B–D). Some CD34 positive EC as well as some RPE cells did not express E-selectin (Fig. 3B–D). CD 105 expressing EC were not always E-selectin positive (Fig. 3A,B).

Hematoxylin–eosin and PAS staining (Fig. 4A) were performed to determine the histologic orientation and to confirm the location of the diffuse drusen.

CK18 expressing RPE cells were found to be present in all of the CNV samples (Fig. 4B).

Positive staining for endostatin in RPE-Bruch's membrane was found in 50% of the membranes at varying intensities (Figs. 1A and 4C). In some CNV, endostatin expression was not evenly distributed in the RPE cell layer but was only partially expressed. Positive immunostaining in vessels was observed in 72% of the specimens (Figs. 1A and 4C–F). Endostatin staining in CNV specimens also persisted after bleaching of the specimen for melanin (Fig. 4D). Vessels in a CNV were only partially stained for endostatin (Fig. 4E). A few vessels expressing CD105 but no endostatin were detected. Endostatin expressing vessels were not always E-selectin positive (Figs. 3B and 4E). Staining intensity between vessels in the same CNV also varied. Endostatin staining was also observed in stromal cells and in fibrous stroma itself (Fig. 4F).

Endostatin and E-selectin were co-expressed in many CNV specimens (Figs. 3C,D and 4C,D). However, expression of endostatin in RPE-Bruch's membrane, vessels and stroma evaluated separately or as "the overall expression score" were not correlated with the corresponding E-selectin expression in CNV membranes ($p = 0.3482$, $\rho = 0.3130$; $p = 0.6294$, $\rho = -0.1610$; $p = 0.5658$, $\rho = -0.1820$; $p = 0.3978$, $\rho = -0.2670$, respectively)

In CNV, VEGF staining was absent in RPE cells of 53% of the specimens. When expressed, VEGF staining intensity in RPE varied from weak to strong. Similarly, VEGF expression in EC was seen in 55% of the CNV. Weak to moderate expression was found in 17% and 28% of the examined membranes, respectively. In 86% of the cases, VEGF expression could be

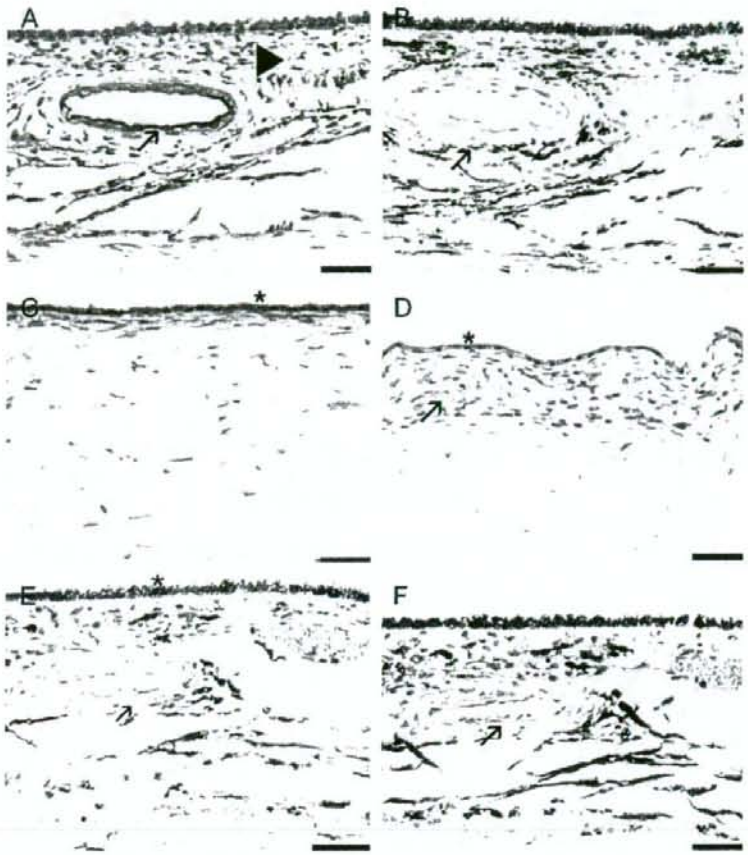


Fig. 2. Immunohistochemistry of a control eye (Case 4 in Table 1) probed with an antibody against endostatin (A, C, D), E-selectin (E) and VEGF (F). Sections were stained with either red alkaline phosphatase substrate (A–D, F) or AEC chromogen (E) and counterstained with hematoxylin. (A) Some vessels within the choroid disclose a prominent staining (arrow) whereas others are completely negative (arrowhead). (B) A serial section from the same specimen is used as a negative control by omitting the primary antibody "endostatin". None of the choroidal structures display false positive staining. (C) Endostatin labelling is present in part of the RPE-Bruch's membrane complex (*) whereas endostatin negative RPE-Bruch's membrane complex is also seen in the same eye (D, *). (D) A weakly stained choroidal vessel is apparent in the same section (arrow). (E) E-selectin is not expressed in any of the structures of the same eye (*:RPE, arrow:vessel) whereas VEGF is expressed weakly in some of the choroidal vessels (F, arrow). Scale bar: 50 μm.

encountered within the stroma of the membranes, especially in fibroblast-like and inflammatory cells (Figs. 1C and 5A). CNV membranes and vessels strongly stained both for VEGF and endostatin were also present (Figs. 4F and 5A).

### *3.3. Ki-67 labelling, proliferative and inflammatory activity in CNV*

In CNV, a differing number of Ki-67 positive proliferating cells were detected. Ki-67 positive cells ($n = 971$) was rarely EC ($n = 51$, 5.3%) or RPE cells ($n = 36$, 3.7%) but mostly appeared to belong to stromal cells ($n = 874$, 90%), especially inflammatory infiltrate (Fig. 5B).

Proliferative activity in CNV membranes varied strongly from 0 to 514.01 nuclei/mm$^2$ (median 55.13, mean 105.72, SE 24.71). When "overall endostatin staining score" was concerned, there was no statistically significant difference in the median proliferative activity between the group with the high endostatin staining score (median 59.7, SE 31.67 overall, endostatin score 5–9, $n = 18$) and with the lower one (median 43.3, SE 38.88, overall endostatin staining score <5, $n = 18$) ($p = 0.4961$). High proliferative activity was observed in some CNV with strong endostatin expression (Figs. 4F and 5B). No correlation was found between the proliferative activity and the overall endostatin staining by Spearman's coefficient correlation test ($p = 0.321$, $\rho = 0.159$). Proliferative activity was also not correlated with either "E-selectin overall staining score" ($p = 0.622$, $\rho = 0.092$) or "VEGF overall staining score" ($p = 0.659$, $\rho = -0.075$).

Of the 36 CNV, 64% (23/36) was classified as inflammatory active (IA) whereas 36% (13/36) of the specimens were inflammatory inactive (II). There was no statistically significant

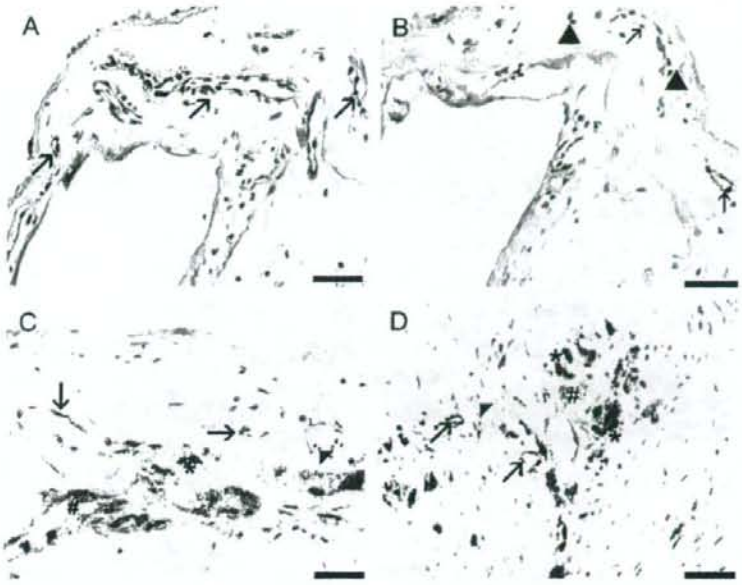


Fig. 3. Immunohistochemistry of the three different CNV membranes probed with antibodies against CD105 (A) and E-selectin (B–D). Sections were stained with 3-diaminobenzidine (A) and AEC (B–D) resulting in a brown and red chromogen, respectively and counterstained with hematoxylin. (A) CD105 is selectively expressed in endothelial cells (arrows). (B) CD105 expressing vessels do not always express E-selectin. Arrowheads point to some of the E-selectin negative vessels expressing CD105 in the parallel section (A). (B–D) E-selectin is positive in some but not all RPE cells and vascular endothelial cells. Arrows and asterisks indicate E-selectin expressing EC and RPE cells, respectively. However, in the same specimens, some RPE cells (#) and EC (arrowheads) are E-selectin negative. Scale bar: 50 μm.

difference either in endostatin staining intensity of RPE-Bruch's membrane (median 1, $p = 0.0789$), vessels (median 3, $p = 0.9715$), stroma (median 1, $p = 0.0719$) when evaluated separately (range 0–3) or in the "overall endostatin staining score" (median 5, range 0–9, $p = 0.1727$) between IA and II CNV. Similarly, E-selectin staining intensity in RPE-Bruch's membrane complex, vessels, and stroma evaluated separately (range 0–3) as well as the "E-selectin overall staining score" (range 0–9) did not vary significantly between IA (median 1, 0, 0, 3, respectively) and II membranes (median 1, 0, 0, 2; $p = 0.922$, $p = 0.8946$, $p = 0.9171$, $p = 0.7928$, respectively). Furthermore, in II CNV, VEGF expression either in RPE cells, vessels and stroma evaluated separately (median 0, 1, 2, respectively, range 0–3 for all) or in terms of "overall VEGF staining score" (median 4, range 0–9) were also not significantly different from those in IA CNV (median 0, 1, 2, 3; $p = 0.8428$, $p = 0.7274$, $p = 0.7119$, $p = 0.6657$, respectively).

However, the proliferative activity in IA CNV (median 72.89, range 0–514.081, mean 149.125, SE 35.4) was significantly higher than in II CNV (median 12.85 nuclei/mm$^2$, range 0–113.693, mean 28.931, SE 12.85) ($p = 0.0059$).

## 4. Discussion

Endothelial cell activation, proliferation, tube formation and development of the basement membrane are among the successive steps during neovascularization (Pepper, 2001). Numerous angiogenesis stimulating factors such as VEGF are involved in this process. The effects of angiogenesis activators are balanced by angiogenesis inhibitors such as endostatin. Herein, we aimed to evaluate the presence and co-expression of endostatin with other markers representing different aspects of the process in order to understand the role of this endogenous inhibitor in the pathogenesis of CNV.

Collagen XVIII is a component of Bruch's membrane as well as the basement membrane of both active and quiescent vessels. In contrast, endostatin was shown to be selectively expressed in newly formed vessels in pathological angiogenesis but not in the quiescent vessels of some non-angiogenic and/or non-pathologic control organs other than eye (Ergun et al., 2001). However, in our series, similar to the findings of Bhutto et al. (2004), endostatin was expressed in the RPE-Bruch's membrane complex and choriocapillaris of some apparently normal control eyes, even in those from young donors. In order to evaluate further if endostatin was positive only in vessels lined by activated EC in CNV, we examined the expression of CD105, a marker for activated/proliferating EC (Grisanti et al., 2004). Although vessels were mostly expressing both of them, it was still possible to detect a few vessels stained for only one of the markers. Additionally, some endostatin expressing vessels were not positively stained for E-selectin which is expressed in proliferating EC under non-inflammatory conditions (Luo et al., 1999). Moreover,

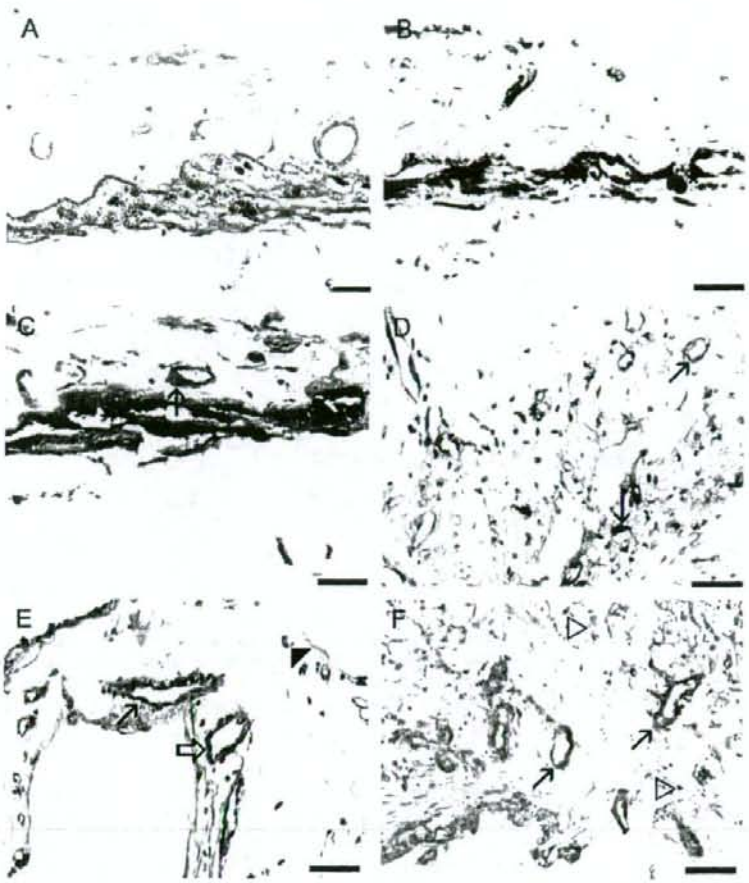


Fig. 4. Serial sections from those specimens in Fig. 3 (A-E) and another CNV (F). Sections are stained with PAS (A) or probed with antibodies against cytokeratin18 (B), endostatin (C–F). (A) PAS staining helps the overall orientation of the specimen. (B) RPE cells express Cytokeratin18 (*) in the same membrane. (C–F) RPE-Bruch's membrane complex (*) as well as vessels (arrows) are strong endostatin positive. (C, D) The specimens stained for E-selectin in Fig. 3C and D are also strong positive for endostatin in the serial sections. (D) Endostatin immunoreactivity is still detected after bleaching of the specimen for melanin. (E) Endostatin positive vessels (arrows) as well as endostatin negative vessels (arrowhead) are seen in the same specimen. Some endostatin positive vessels (white arrow) are not E-selectin positive as shown in the parallel section in Fig. 3B. (F) Stromal cells also display endostatin (white arrowhead). Sections were stained with the immunoperoxidase (B) or alkaline phosphatase (C–F) techniques with AEC (B) and red alkaline phosphatase substrate chromogen (C–F) and counterstained with hematoxylin. Scale bar: 50 μm.

the EC in endostatin expressing vessels were not always Ki-67 positive. Therefore, endostatin expression seems not to be limited to the newly formed vessels in the neovascularized tissue when normal choroid and CNV membranes are concerned.

During angiogenesis, activated EC release proteolytic enzymes like MMPs that break up the peptide bonds within the protease sensitive region of collagen XVIII (Lee et al., 2002; Kim et al., 2000). Consequently, local inhibitors of angiogenesis like endostatin fragments are released. Variations in intensity and pattern of endostatin expression in CNV as well as negative or limited staining in some control eyes may be, therefore, due to microenvironmental variations in the level of proteolytic enzymes.

The effect of endostatin on the proliferative activity of EC is still controversial. Contrary to the studies showing its inhibitory effect (Wang et al., 2004; Abdollahi et al., 2003), Skovseth et al. (2005) and Wang et al. (2005) reported that endostatin has no effect on the proliferative activity of the EC although it dramatically inhibits EC migration and perivascular cell recruitment. In our series, in some specimens, proliferative activity was remarkably high in spite of strong endostatin expression. When the CNV membranes were classified according to the "endostatin overall staining score", the difference in proliferative activity was not significant between the group with high (5–9) and low score (<5). In the specimens investigated, the proliferative activity did not seem to be

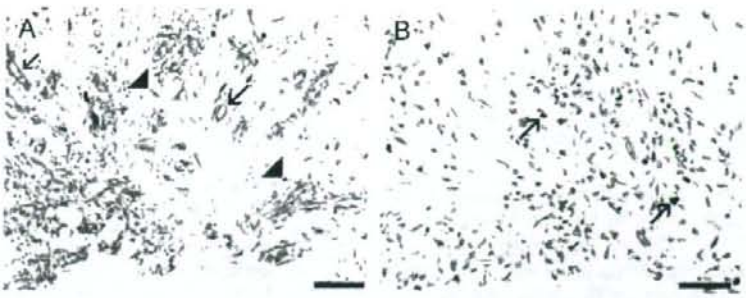


Fig. 5. Immunohistochemistry of serial sections from the CNV specimen shown in Fig. 4F probed with antibodies against VEGF (A) and Ki-67 (B). Sections were stained with red alkaline phosphatase substrate (A) and 3-diaminobenzidine (B) resulting in a red and brown chromogen, respectively, and counterstained with hematoxylin. (A) This specimen displays strong VEGF expression in EC (arrow) and stromal cells (arrowheads) such as fibroblasts and inflammatory cells despite strong endostatin expression shown in the serial section in Fig. 4F. (B) Several Ki-67 positive nuclei are detected (arrows) in this specimen. None of these nuclei appear to be associated with endothelial cells. Scale bar: 50 μm.

correlated with endostatin staining intensity but with inflammation; the Ki-67 positive cells were mostly stromal and inflammatory cells. We detected significantly higher proliferative activity in IA CNV than II CNV; however, there was no significant difference in the endostatin overall staining score between IA and II CNV. Proliferative activity did not seem to correlate with either E-selectin or VEGF expression scores in the CNV.

Collagen XVIII/endostatin was suggested to be critical for normal ocular blood vessel formation, vision and RPE function. Lack of collagen XVIII/endostatin resulted in ocular as well as functional RPE abnormalities with the formation of excess basal laminar-like deposits similar to drusen (Sertie et al., 2000; Marneros et al., 2004; Fukai et al., 2002). Still, it was not clear if collagen XVIII or its endostatin part was functionally important in AMD pathogenesis. Recent studies revealed that the level of endostatin was reduced in Bruch's membrane, RPE basal lamina and choriocapillaris in eyes with AMD whereas collagen XVIII immunostaining was similar in pattern and intensity in comparison to the normal donor eyes. It was concluded that reduced endostatin expression in choroid might be a factor contributing to AMD and perhaps choroidal neovascularization pathogenesis (Bhutto et al., 2004).

In our CNV specimens, E-selectin was detected in RPE and stromal cells as well as EC similar to the observations of others (Yeh et al., 2004; Shen et al., 1998). Interestingly, E-selectin was expressed only in CNV membranes but not in any of the control eyes. This finding is also concordant with the findings from Yeh et al. (2004). Taken together, these observations might point to a possible role of endostatin in CNV pathogenesis as E-selectin was recently suspected to be required for the antiangiogenic activity of endostatin (Yu et al., 2004). Yu et al. showed that in E-selectin −/− mice, FGF-induced corneal angiogenesis and VEGF-stimulated endothelial sprout formation was not inhibited by endostatin and cells were endostatin-resistant in contrast to the normal controls. Our immunohistopathologic evaluation revealed that endostatin is co-expressed with E-selectin in RPE-Bruch's membrane complex, vessels and stroma in CNV membranes where pathological angiogenesis is active but not in either normal control eyes or the eye with early AMD. Endostatin seems to have other physiologic functions in normal eyes as stated by previous reports (Sertie et al., 2000; Marneros et al., 2004; Fukai et al., 2002), but its anti-angiogenic effect in conjunction with E-selectin seems to apply only to CNV membranes.

Angiostatin, another potent inhibitor of angiogenesis was shown to up-regulate E-selectin in proliferating EC, and was, therefore, suggested to be inhibiting selectively the pathological angiogenesis without effects on quiescent endothelium (Luo et al., 1998). However, information concerning such a correlation between endostatin and E-selectin is lacking. In our series, no correlation was found between endostatin and E-selectin expression, but, it should be sought by further experimental studies.

In our specimens, expression of E-selectin, an endothelial specific adhesion molecule especially for leukocytes, did not vary significantly between IA and II CNV membranes. E-selectin, however, is known to be induced not only by inflammatory stimuli but also by the proliferative state of the endothelium in non-inflammatory pathway (Luo et al., 1999). Although no correlation was found between proliferative activity of the membranes and E-selectin expression in our specimens, it must be considered that Ki-67 expressing proliferating cells in CNV were mostly stromal cells but not EC.

Grossniklaus et al. (2002) proposed that the development of CNV membrane is based on a dynamic process with sequential initiation, maintenance and involution stages. There is clinical (Green, 1996) and experimental (Wada et al., 1999) evidence for spontaneous involution of CNV. Grossniklaus et al. suggested that a decreased production of cytokines, especially VEGF, and an increased fibrosis may be responsible for the involution as CNV matures. Besides its inhibitory effect on EC stimulated by VEGF and FGF-2, endostatin was shown to stabilize the newly formed endothelial tubes in the early phase by constructing inter-endothelial junctions and attaching EC to the basement membrane (Ergun et al., 2001; Yu et al., 2004; Dixelius et al., 2002). Endostatin is also known to reduce VEGF induced retinal vascular permeability and neovascularization (Takahashi et al., 2003). Therefore, we suppose that endogenous endostatin expression may participate in

the spontaneous involution of CNV. RPE cells have a dual and regulatory role in CNV pathogenesis. RPE cells may promote progression of CNV in early stages; however, in the late stages, they have been suggested to promote regression (Lutty et al., 1999). The presence of endostatin and E-selectin within the RPE-Bruch's membrane complex in CNV may have a role in the involution process.

Vitreous levels of VEGF and endostatin were shown to be correlated with the activity of angiogenesis in diabetic retinopathy (Noma et al., 2002). In CNV, this may also be the fact but distinct stages of the angiogenesis process within this pathological tissue may act rather concomitantly than subsequently. The collagen XVIII/endostatin system limits its self activation by blocking the activation and the catalytic activity of MMP-2 (Ferreras et al., 2000; Lee et al., 2002). This suggests that angiogenic and antiangiogenic factors are active concomitantly and dependent on each other in CNV until they come into a balance and stabilize. This may explain the concomitant expression of intense VEGF as well as intense endostatin staining within some angiogenic specimens in our series and almost negative expression of endostatin in disciform scars examined by Bhutto et al. (2004).

Experimental trials of exogenous endostatin treatment for CNV have been already conducted and results seem to be promising (Mori et al., 2001). To the best of our knowledge, our results are the first to describe endostatin and E-selectin expression in a relatively high number of CNV membranes. Physiological levels of endostatin expression, although strong, may be insufficient to inhibit the existing CNV totally as is the case in tumors (Fukai et al., 2002). However, endogenous endostatin levels are proven to be increased by orally administered drugs (Folkman, 2004). Therefore, the knowledge gained from our work may underline a new perspective for the future trials in CNV treatment.

The proper interpretation of this study is limited by the fact that age and 'maturity' of the surgically excised CNV specimens cannot be determined accurately. It is, therefore, not possible to determine the onset of endostatin expression according to time and phase of angiogenesis. Nevertheless, it is conceivable that endostatin is among the endogenous antiangiogenic factors expressed in human CNV. Its co-expression with E-selectin in CNV suggests that endostatin may act as an anti-angiogenesis factor in modulating neovascularization in CNV. Therapeutic up-regulation of endostatin as an alternative to its exogenous delivery may be an important strategy in the future treatment of neovascular AMD to stabilize the course of neovascularization.

## Acknowledgements

This work was supported by the Jung Foundation, the Grimmke Foundation, and Vision 100 Foundation.

## References

Abdollahi, A., Lipson, K.E., Sckell, A., Zieher, H., Klenke, F., Poerschke, D., Roth, A., Han, X., Krix, M., Bischof, M., Hahnfeldt, P., Grone, H.J., Debus, J., Hlatky, L., Huber, P.E., 2003. Combined therapy with direct and indirect angiogenesis inhibition results in enhanced antiangiogenic and antitumor effects. Cancer Res. 63, 8890–8898.

Abdollahi, A., Hahnfeldt, P., Maercker, C., Grone, H.J., Debus, J., Ansorge, W., Folkman, J., Hlatky, L., Huber, P.E., 2004. Endostatin's antiangiogenic signaling network. Mol. Cells 13, 649–663.

Amin, R., Pulkin, J.E., Frank, R.N., 1994. Growth factor localization in choroidal neovascular membranes of age-related macular degeneration. Invest. Ophthalmol. Vis. Sci. 35, 3178–3188.

Auricchio, A., Behling, K.C., Maguire, A.M., O'Connor, E.M., Bennett, J., Wilson, J.M., Tolentino, M.J., 2002. Inhibition of retinal neovascularization by intraocular viral-mediated delivery of anti-angiogenic agents. Mol. Ther 6, 490–494.

Bhutto, I.A., Kim, S.Y., McLeod, D.S., Merges, C., Fukai, N., Olsen, B.R., Lutty, A., 2004. Localization of collagen XVIII and the endostatin portion of collagen XVIII in aged human control eyes and eyes with age-related macular degeneration. Invest. Ophthalmol. Vis. Sci. 45, 1544–1552.

Dhanabal, M., Ramchandran, R., Waterman, M.J., Lu, H., Knebelmann, B., Segal, M., Sukhatme, V.P., 1999. Endostatin induces endothelial cell apoptosis. J. Biol. Chem. 274, 11721–11726.

Dixelius, J., Larsson, H., Sasaki, T., Holmqvist, K., Lu, L., Engstrom, A., Timpl, R., Welsh, M., Claesson-Welsh, L., 2000. Endostatin-induced tyrosine kinase signaling through the Shb adaptor protein regulates endothelial cell apoptosis. Blood 95, 3403–3411.

Dixelius, J., Cross, M., Matsumoto, T., Sasaki, T., Timpl, R., Claesson-Welsh, L., 2002. Endostatin regulates endothelial cell adhesion and cytoskeletal organization. Cancer Res. 62, 1944–1947.

Ergun, S., Kilic, N., Wurmbach, J.H., Ebrahimnejad, A., Fernando, M., Sevinc, S., Kilic, E., Chalajour, F., Fiedler, W., Lauke, H., Lamszus, K., Hammerer, P., Weil, J., Herbst, H., Folkman, J., 2001. Endostatin inhibits angiogenesis by stabilization of newly formed endothelial tubes. Angiogenesis 4, 193–206.

Eriksson, K., Magnusson, P., Dixelius, J., Claesson-Welsh, L., Cross, M.J., 2003. Angiostatin and endostatin inhibit endothelial cell migration in response to FGF and VEGF without interfering with specific intracellular signal transduction pathways. FEBS Lett. 536, 19–24.

Folkman, J., 2004. Endogenous angiogenesis inhibitors, 2004. APMIS 112 (7–8), 496–507.

Ferreras, M., Felbor, U., Lenhard, T., Olsen, B.R., Delaisse, J., 2000. Generation and degradation of human endostatin proteins by various proteinases. FEBS Lett. 486, 247–251.

Fukai, N., Eklund, L., Marneros, A.G., Oh, S.P., Keene, D.R., Tamarkin, L., Niemela, M., Ilves, M., Li, E., Pihlajaniemi, T., Olsen, B.R., 2002. Lack of collagen XVIII/endostatin results in eye abnormalities. EMBO J 21, 1535–1544.

Green, W.R., 1996. The retina. In: Spencer, W.H. (Ed.), Ophthalmic Pathology: An Atlas and Textbook. WB Saunders, Philadelphia, pp. 982–1051.

Grisanti, S., Canbek, S., Kaiserling, E., Adam, A., Lafaut, B., Gelisken, F., Szurman, P., Henke-Fahle, S., Oficjalska-Mlynczak, J., Bartz-Schmidt, K.U., 2004. Expression of endoglin in choroidal neovascularization. Exp. Eye. Res. 78, 207–213.

Grossniklaus, H.E., Ling, J.X., Wallace, T.M., Dithmar, S., Lawson, D.H., Cohen, C., Elner, V.M., Elner, S.G., Sternberg Jr., P., 2002. Macrophage and retinal pigment epithelium expression of angiogenic cytokines in choroidal neovascularization. Mol. Vis 21, 119–126.

Kim, Y.M., Jang, J.W., Lee, O.H., Yeon, J., Choi, E.Y., Kim, K.W., Lee, S.T., Kwon, Y.G., 2000. Endostatin inhibits endothelial and tumor cellular invasion by blocking the activation and catalytic activity of matrix metalloproteinase 2. Cancer Res. 60, 5410–5413.

Kivela, T., 1995. Immunohistochemical staining followed by bleaching of melanin: a practical method for ophthalmic pathology. Br. J. Biomed. Sci. 52, 325–326.

Kvanta, A., Algvere, P.V., Berglin, L., Seregard, S., 1996. Subfoveal fibrovascular membranes in age-related macular degeneration express vascular endothelial growth factor. Invest. Ophthalmol. Vis. Sci. 37, 1929–1934.

Lambert, V., Wielockx, B., Munaut, C., Galopin, C., Jost, M., Itoh, T., Werb, Z., Baker, A., Libert, C., Krell, H.W., Foidart, J.M., Noel, A.,

Rakic, J.M., 2003. MMP-2 and MMP-9 synergize in promoting choroidal neovascularization. FASEB J. 17, 2290–2292.

Lanzer, R.C., Raff, M.C., 1987. Astrocytes induce blood-brain barrier properties in endothelial cells. Nature 325, 253–257.

Lee, S.J., Jang, J.W., Kim, Y.M., Lee, H.I., Jeon, J.Y., Kwon, Y.G., Lee, S.T., 2002. Endostatin binds to the catalytic domain of matrix metalloproteinase-2. FEBS Lett. 519, 147–152.

Luo, J., Lin, J., Paranya, G., Bischoff, J., 1998. Angiostatin upregulates E-selectin in proliferating endothelial cells. Biochem. Biophys. Res. Commun 245 (3), 906–911.

Luo, J., Paranya, G., Bischoff, J., 1999. Noninflammatory expression of E-selectin is regulated by cell growth. Blood 93, 3785–3791.

Lutty, G., Grunwald, J., Majji, A.B., Uyama, M., Yoneya, S., 1999. Changes in choriocapillaris and retinal pigment epithelium in age-related macular degeneration. Mol. Vis. 5, 35.

Makitie, T., Tarkkanen, A., Kivela, T., 1998. Comparative immunohistochemical oestrogen receptor analysis in primary and metastatic uveal melanoma. Graefes Arch. Clin. Exp. Ophthalmol. 236, 415–419.

Marneros, A.G., Keene, D.R., Hansen, U., Fukai, N., Moulton, K., Goletz, P.L., Moiseyev, G., Pawlyk, B.S., Halfter, W., Dong, S., Shibata, M., Li, T., Crouch, R.K., Bruckner, P., Olsen, B.R., 2004. Collagen XVIII/endostatin is essential for vision and retinal pigment epithelial function. EMBO J. 14, 89–99.

Martin, G., Schlunck, G., Hansen, L.L., Agostini, H.T., 2004. Differential expression of angioregulatory factors in normal and CNV-derived human retinal pigment epithelium. Graefes Arch. Clin. Exp. Ophthalmol. 242, 321–326.

Mori, K., Ando, A., Gehlbach, P., Nesbitt, D., Takahashi, K., Goldsteen, D., Penn, M., Chen, C.T., Mori, K., Melia, M., Phipps, S., Moffat, D., Brazzell, K., Liau, G., Dixon, K.H., Campochiaro, P.A., 2001. Inhibition of choroidal neovascularization by intravenous injection of adenoviral vectors expressing secretable endostatin. Am. J. Pathol. 159, 313–320.

Noma, H., Funatsu, H., Yamashita, H., Kitano, S., Mishima, H.K., Hori, S., 2002. Regulation of angiogenesis in diabetic retinopathy: possible balance between vascular endothelial growth factor and endostatin. Arch. Ophthalmol. 120, 1075–1080.

O'Reilly, M.S., Boehm, T., Shing, Y., Fukai, N., Vasios, G., Lane, W.S., Flynn, E., Birkhead, J.R., Olsen, B.R., Folkman, J., 1997. Endostatin: an endogenous inhibitor of angiogenesis and tumor growth. Cell 88, 277–285.

Pepper, M.S., 2001. Role of the matrix metalloproteinase and plasminogen activator-plasmin systems in angiogenesis. Arterioscler. Thromb. Vasc. Biol. 21. 1104–1017.

Sasaki, T., Fukai, N., Mann, K., Gohring, W., Olsen, B.R., Timpl, R., 1998. Structure, function and tissue forms of the C-terminal globular domain of collagen XVIII containing the angiogenesis inhibitor endostatin. EMBO J. 17, 4249–4256.

Sertie, A.L., Sossi, V., Camargo, A.A., Zatz, M., Brahe, C., Passos-Bueno, M.R., 2000. Collagen XVIII, containing an endogenous inhibitor of angiogenesis and tumor growth, plays a critical role in the maintenance of retinal structure and in neural tube closure (Knobloch syndrome). Hum. Mol. Genet. 9, 2051–2058.

Shen, W.Y., Yu, M.J., Barry, C.J., Constable, I.J., Rakoczy, P.E., 1998. Expression of cell adhesion molecules and vascular endothelial growth factor in experimental choroidal neovascularisation in the rat. Br. J. Ophthalmol. 82, 1063–1071.

Skovseth, D.K., Veuger, M.J., Sorensen, D.R., De Angelis, P.M., Haraldsen, G., 2005. Endostatin dramatically inhibits endothelial cell migration, vascular morphogenesis and perivascular cell recruitment in vivo. Blood 105, 1044–1051.

Takahashi, K., Saishin, Y., Saishin, Y., Silva, R.L., Oshima, Y., Oshima, S., Melia, M., Paszkiet, B., Zerby, D., Kadan, M.J., Liau, G., Kaleko, M., Connelly, S., Luo, T., Campochiaro, P.A., 2003. Intraocular expression of endostatin reduces VEGF-induced retinal vascular permeability, neovascularization, and retinal detachment. FASEB J. 17, 896–898.

The Macular Photocoagulation Study Group, 1991. Argon laser photocoagulation for neovascular maculopathy: five year results from randomized clinical trials. Arch. Ophthalmol. 109, 1109–1114.

Wada, M., Ogata, N., Otsuji, T., Uyama, M., 1999. Expression of vascular endothelial growth factor and its receptor (KDR/ffk-1) mRNA in experimental choroidal neovascularization. Curr. Eye Res. 18, 203–213.

Wang, W., Niu, X.G., Xie, L.X., Dong, X.G., 2004. Liposomes mediated plasmids encoding human endostatin inhibits endothelial cell proliferation. Zhonghua Yan Ke. Za. Zhi. 40, 321–325.

Wang, Y.S., Eichler, W., Friedrichs, U., Yafai, Y., Hoffmann, S., Yasukawa, T., Hui, Y.N., Wiedemann, P., 2005. Impact of endostatin on bFGF-induced proliferation, migration, and matrix metalloproteinase-2 expression/secretion of bovine choroidal endothelial cells. Curr. Eye Res. 30, 479–489.

Yamaguchi, N., Anand-Apte, B., Lee, M., Sasaki, T., Fukai, N., Shapiro, R., Que, I., Lowik, C., Timpl, R., Olsen, B.R., 1999. Endostatin inhibits VEGF-induced endothelial cell migration and tumor growth independently of zinc binding. EMBO J 18, 4414–4423.

Yeh, D.C., Bula, D.V., Miller, J.W., Gragoudas, E.S., Arroyo, J.G., 2004. Expression of leukocyte adhesion molecules in human subfoveal choroidal neovascular membranes treated with and without photodynamic therapy. Invest. Ophthalmol. Vis. Sci. 45, 2368–2373.

Yu, Y., Moulton, K.S., Khan, M.K., Vineberg, S., Boye, E., Davis, V.M., O'Donnell, P.E., Bischoff, J., Milstone, D.S., 2004. E-selectin is required for the antiangiogenic activity of endostatin. Proc. Natl. Acad. Sci. USA 101, 8005–8010.

Zatterstrom, U.K., Felbor, U., Fukai, N., Olsen, B.R., 2000. Collagen XVIII/endostatin structure and functional role in angiogenesis. Cell Struct. Funct. 25, 97–101.

# Consequences of Verteporfin Photodynamic Therapy on Choroidal Neovascular Membranes

*Olcay Tatar, MD; Edwin Kaiserling, MD; Annemarie Adam, Faik Gelisken, MD; Kei Shinoda, MD, PhD; Michael Völker MD; Bart A. Lafaut, MD; Karl Ulrich Bartz-Schmidt, MD; Salvatore Grisanti, MD*

**Objective:** To examine the impact of photodynamic therapy (PDT) on angiogenesis in human choroidal neovascular membranes with respect to vascular endothelial growth factor (VEGF) expression, proliferation, and vascularization.

**Methods:** Retrospective review of an interventional case series of 50 patients (50 eyes) who underwent removal of choroidal neovascular membranes. Choroidal neovascularization was secondary to age-related macular degeneration. Twenty patients were treated with PDT 3 to 655 days before surgery. Choroidal neovascular membranes were stained for CD34, CD105, Ki-67, cytokeratin 18, and VEGF. Thirty choroidal neovascular membranes secondary to age-related macular degeneration without previous treatment were used as controls.

**Results:** Specimens without pretreatment disclosed varying degrees of vascularization, proliferative activity, and VEGF expression by different cells. Specimens treated with PDT 3 days earlier showed mostly occluded vessels, damaged endothelial cells, and low proliferative activity. In contrast, specimens excised at later time points after PDT were highly vascularized and proliferating. This chronology was associated with an impressive VEGF immunoreactivity unique to retinal pigment epithelial cells shortly after PDT that also shifted to other cells at later time points.

**Conclusions:** Photodynamic therapy induces selective vascular damage in choroidal neovascular membranes. The effectiveness and selectivity of this treatment, however, seem to be jeopardized by a rebound effect initiated by enhanced VEGF expression in retinal pigment epithelial cells.

*Arch Ophthalmol 2006;124:815-823*

AGE-RELATED MACULAR DEgeneration (AMD) is the leading cause of legal blindness in patients older than 60 years in the Western world.[1,2] The exudative form of the disease is characterized by the development of choroidal neovascularization (CNV) in the macular area that leads to irreversible damage to the neurosensory retina and severe loss of visual acuity. Numerous treatment modes have been attempted to destroy the pathological blood vessels using thermal photocoagulation, ionizing radiation, or photosensitizing dyes or to surgically remove the neovascular tissue with or without replacement of the damaged retinal pigment epithelium (RPE) or translocation of the fovea. Although some modalities are still experimental, large randomized clinical trials have shown the value of laser photocoagulation and photodynamic therapy (PDT). The major handicap of laser photocoagulation, however, is the inevitable damage to the neurosensory retina that is associated with a sudden decrease in visual acuity. This problem was overcome by the introduction of PDT.

Photodynamic therapy is a nonthermal process based on the targeted photoactivation of an intravenously administered photosensitive drug. The activated dye results in the creation of oxygen intermediates and free radicals affecting the exposed endothelial cells. Photodynamic therapy seems to be an ideal treatment approach for CNV, allowing selective photothrombosis of CNV without damage to the overlying neurosensory retina.

After randomized clinical trials demonstrated that PDT with verteporfin (Visudyne; Novartis AG, Buelach, Switzerland) is an effective treatment for subfoveal CNV secondary to AMD, it was accepted as a routine procedure under certain circumstances.[3-8] The potential and success of verteporfin PDT, however, are considerably compromised by a recurrence rate of about 90% within 3 months and a mean visual acuity loss of 2 Early Treatment Diabetic Retinopathy Study lines within 6 months.[3]

Author Affiliations: University Eye Clinic at the Centre for Ophthalmology, Eberhard-Karls-University (Drs Tatar, Gelisken, Völker, Bartz-Schmidt, and Grisanti) and Department of Pathology, University of Tübingen (Dr Kaiserling and Ms Adam), Tübingen, Germany; Laboratory of Visual Physiology, National Institute of Sensory Organs, Tokyo, Japan (Dr Shinoda); and Department of Ophthalmology, AZ StJan, Bruges, Belgium (Dr Lafaut).